damage of neuronal cells. Moreover, genetic suppression of the pathogenic AR–induced upregulation of CGRP1 mitigated neuronal damage in mice. Our findings thus indicate that increased expression of CGRP1 contributes to motor neuron degeneration in SBMA.

CGRP1 is a multifunctional neuropeptide that has a potent vasodilatory effect and is believed to have a key role in vascular headaches[24]. In the nervous system, CGRP1 is also known to regulate nociceptor activation, neuroinflammation and neuronal nicotinic receptor functions[38,39]. Our study shows that overexpression of CGRP1 induces cytotoxicity in neuronal cells, and deletion of *Calca* ameliorates motor neuron damage in the mouse model of SBMA. We also found that pathogenic AR activates the JNK pathway via upregulation of CGRP1 in cellular and mouse models of SBMA. In agreement with our results, CGRP1 was previously shown to activate the JNK pathway in neuroblastoma cells[40]. In addition, we have found that activation of the JNK pathway enhances neuronal damage and that pharmacological inhibition of JNK mitigates the toxicity of pathogenic AR in neuronal cells. Abnormal activation of the JNK pathway has also been implicated in the pathogenesis of neurodegenerative disorders, including SBMA[32,41–44].

On the basis of its potent effects on neuroinflammation, CGRP1 has been identified as a therapeutic target for migraines[45]. Agonists of the 5-HT1B/1D receptor, which are clinically used for the suppression of migraines, reduce the serum levels of CGRP1 (ref. 29). Here we showed that the antimigraine drug naratriptan and other 5-HT1B/1D receptor agonists reduce promoter activity of the gene encoding CGRP1 and decrease mRNA levels of *CALCA* in neuronal cells via the induction of DUSP1. Oral administration of naratriptan also decreased the expression of Cgrp1 and ameliorated the motor impairment in a mouse model of SBMA. Furthermore, our study also showed that naratriptan treatment inhibits the JNK pathway in cellular and mouse models of SBMA. These observations indicate that stimulation of the 5-HT1B/1D receptor suppresses the neurotoxicity of polyglutamine-expanded AR by downregulating CGRP1 resulting in inactivation of the JNK pathway. As naratriptan is widely used in patients with migraine, this drug is a potential candidate for SBMA therapy. However, the efficacy awaits further clinical trials in patients given the limited efficacy of androgen ablation trials, despite the complete suppression of neurodegeneration in AR-97Q mice by leuprorelin[25,46,47]. As naratriptan showed limited effects on survival and motor function in the SBMA model mice, further studies are needed to evaluate the efficacy and safety of long-term treatment with naratriptan in humans.

METHODS

Methods and any associated references are available in the online version of the paper.

Accession codes. Microarray data have been deposited in the Gene Expression Omnibus (GEO) with accession code GSE39865.

Note: Supplementary information is available in the online version of the paper.

ACKNOWLEDGMENTS

This work was supported by a Center-of-Excellence grant, a Grant-in-Aid for Scientific Research on Innovated Areas "Foundation of Synapse and Neurocircuit Pathology" (No. 22110005) and Grants-in-Aid from the Ministry of Education, Culture, Sports, Science and Technology, Japan (Nos. 21229011, 21689024 and 23390230); grants from the Ministry of Health, Labor and Welfare, Japan; Core Research for Evolutional Science and Technology (CREST) from Japan Science and Technology Agency (JST); and a grant from the Kennedy Disease Association.

AUTHOR CONTRIBUTIONS

Project planning was performed by M.M., M.K., H.K. and G.S.; microarray analysis by M.M. and M.K.; cellular analysis by M.M., M.K., H.A., H.D., S.M. and Y.M.; primary motor neuron culture by M.K., S.I. and Y.F.; animal work by M.M., M.K., N.K. and M.I.; tissue staining by M.M., M.K. and M.I.; and data analysis by M.M., M.K., F.T. and G.S. M.M. and M.K. drafted the manuscript, and F.T., H.K. and G.S. revised it critically for intellectual content.

COMPETING FINANCIAL INTERESTS

The authors declare no competing financial interests.

Published online at http://www.nature.com/doifinder/10.1038/nm.2932.
Reprints and permissions information is available online at http://www.nature.com/reprints/index.html.

1. Ross, C.A. & Tabrizi, S.J. Huntington's disease: from molecular pathogenesis to clinical treatment. *Lancet Neurol.* **10**, 83–98 (2011).
2. Gatchel, J.R. & Zoghbi, H.Y. Diseases of unstable repeat expansion: mechanisms and common principles. *Nat. Rev. Genet.* **6**, 743–755 (2005).
3. Finsterer, J. Perspectives of Kennedy's disease. *J. Neurol. Sci.* **298**, 1–10 (2010).
4. Katsuno, M. *et al.* Pathogenesis, animal models and therapeutics in spinal and bulbar muscular atrophy (SBMA). *Exp. Neurol.* **200**, 8–18 (2006).
5. La Spada, A.R., Wilson, E.M., Lubahn, D.B., Harding, A.E. & Fischbeck, K.H. Androgen receptor gene mutations in X-linked spinal and bulbar muscular atrophy. *Nature* **352**, 77–79 (1991).
6. Schmidt, B.J., Greenberg, C.R., Allingham-Hawkins, D.J. & Spriggs, E.L. Expression of X-linked bulbospinal muscular atrophy (Kennedy disease) in two homozygous women. *Neurology* **59**, 770–772 (2002).
7. Sobue, G. *et al.* X-linked recessive bulbospinal neuronopathy. A clinicopathological study. *Brain* **112**, 209–232 (1989).
8. Adachi, H. *et al.* Widespread nuclear and cytoplasmic accumulation of mutant androgen receptor in SBMA patients. *Brain* **128**, 659–670 (2005).
9. Bauer, P.O. & Nukina, N. The pathogenic mechanisms of polyglutamine diseases and current therapeutic strategies. *J. Neurochem.* **110**, 1737–1765 (2009).
10. Shao, J. & Diamond, M.I. Polyglutamine diseases: emerging concepts in pathogenesis and therapy. *Hum. Mol. Genet.* **16 Spec No. 2**, R115–R123 (2007).
11. Katsuno, M. *et al.* Testosterone reduction prevents phenotypic expression in a transgenic mouse model of spinal and bulbar muscular atrophy. *Neuron* **35**, 843–854 (2002).
12. Takeyama, K. *et al.* Androgen-dependent neurodegeneration by polyglutamine-expanded human androgen receptor in *Drosophila*. *Neuron* **35**, 855–864 (2002).
13. Nedelsky, N.B. *et al.* Native functions of the androgen receptor are essential to pathogenesis in a *Drosophila* model of spinobulbar muscular atrophy. *Neuron* **67**, 936–952 (2010).
14. Minamiyama, M. *et al.* Sodium butyrate ameliorates phenotypic expression in a transgenic mouse model of spinal and bulbar muscular atrophy. *Hum. Mol. Genet.* **13**, 1183–1192 (2004).
15. Katsuno, M. *et al.* Reversible disruption of dynactin 1–mediated retrograde axonal transport in polyglutamine-induced motor neuron degeneration. *J. Neurosci.* **26**, 12106–12117 (2006).
16. Ranganathan, S. *et al.* Mitochondrial abnormalities in spinal and bulbar muscular atrophy. *Hum. Mol. Genet.* **18**, 27–42 (2009).
17. Katsuno, M. *et al.* Disrupted transforming growth factor-β signaling in spinal and bulbar muscular atrophy. *J. Neurosci.* **30**, 5702–5712 (2010).
18. Steffan, J.S. *et al.* Histone deacetylase inhibitors arrest polyglutamine-dependent neurodegeneration in *Drosophila*. *Nature* **413**, 739–743 (2001).
19. Butler, R. & Bates, G.P. Histone deacetylase inhibitors as therapeutics for polyglutamine disorders. *Nat. Rev. Neurosci.* **7**, 784–796 (2006).
20. Luthi-Carter, R. *et al.* Decreased expression of striatal signaling genes in a mouse model of Huntington's disease. *Hum. Mol. Genet.* **9**, 1259–1271 (2000).
21. Obrietan, K. & Hoyt, K.R. CRE-mediated transcription is increased in Huntington's disease transgenic mice. *J. Neurosci.* **24**, 791–796 (2004).
22. Sugars, K.L. & Rubinsztein, D.C. Transcriptional abnormalities in Huntington disease. *Trends Genet.* **19**, 233–238 (2003).
23. Mo, K. *et al.* Microarray analysis of gene expression by skeletal muscle of three mouse models of Kennedy disease/spinal bulbar muscular atrophy. *PLoS ONE* **5**, e12922 (2010).
24. Ho, T.W., Edvinsson, L. & Goadsby, P.J. CGRP and its receptors provide new insights into migraine pathophysiology. *Nat. Rev. Neurol.* **6**, 573–582 (2010).
25. Katsuno, M. *et al.* Leuprorelin rescues polyglutamine-dependent phenotypes in a transgenic mouse model of spinal and bulbar muscular atrophy. *Nat. Med.* **9**, 768–773 (2003).
26. Popper, P. & Micevych, P.E. The effect of castration on calcitonin gene–related peptide in spinal motor neurons. *Neuroendocrinology* **50**, 338–343 (1989).
27. Ma, W. *et al.* Localization and modulation of calcitonin gene-related peptide-receptor component protein-immunoreactive cells in the rat central and peripheral nervous systems. *Neuroscience* **120**, 677–694 (2003).
28. Walker, C.S., Conner, A.C., Poyner, D.R. & Hay, D.L. Regulation of signal transduction by calcitonin gene–related peptide receptors. *Trends Pharmacol. Sci.* **31**, 476–483 (2010).

29. Durham, P.L. & Russo, A.F. New insights into the molecular actions of serotonergic antimigraine drugs. *Pharmacol. Ther.* **94**, 77–92 (2002).
30. Jhee, S.S., Shiovitz, T., Crawford, A.W. & Cutler, N.R. Pharmacokinetics and pharmacodynamics of the triptan antimigraine agents: a comparative review. *Clin. Pharmacokinet.* **40**, 189–205 (2001).
31. Durham, P.L. & Russo, A.F. Serotonergic repression of mitogen-activated protein kinase control of the calcitonin gene–related peptide enhancer. *Mol. Endocrinol.* **12**, 1002–1009 (1998).
32. Morfini, G. *et al.* JNK mediates pathogenic effects of polyglutamine-expanded androgen receptor on fast axonal transport. *Nat. Neurosci.* **9**, 907–916 (2006).
33. Serra, H.G. *et al.* Gene profiling links SCA1 pathophysiology to glutamate signaling in Purkinje cells of transgenic mice. *Hum. Mol. Genet.* **13**, 2535–2543 (2004).
34. Becanovic, K. *et al.* Transcriptional changes in Huntington disease identified using genome-wide expression profiling and cross-platform analysis. *Hum. Mol. Genet.* **19**, 1438–1452 (2010).
35. Zheng, L.F. *et al.* Calcitonin gene–related peptide dynamics in rat dorsal root ganglia and spinal cord following different sciatic nerve injuries. *Brain Res.* **1187**, 20–32 (2008).
36. Ringer, C., Weihe, E. & Schutz, B. Calcitonin gene–related peptide expression levels predict motor neuron vulnerability in the superoxide dismutase 1–G93A mouse model of amyotrophic lateral sclerosis. *Neurobiol. Dis.* **45**, 547–554 (2012).
37. Ringer, C., Weihe, E. & Schutz, B. Pre-symptomatic alterations in subcellular betaCGRP distribution in motor neurons precede astrogliosis in ALS mice. *Neurobiol. Dis.* **35**, 286–295 (2009).
38. Di Angelantonio, S., Giniatullin, R., Costa, V., Sokolova, E. & Nistri, A. Modulation of neuronal nicotinic receptor function by the neuropeptides CGRP and substance P on autonomic nerve cells. *Br. J. Pharmacol.* **139**, 1061–1073 (2003).
39. Benemei, S., Nicoletti, P., Capone, J.A. & Geppetti, P. Pain pharmacology in migraine: focus on CGRP and CGRP receptors. *Neurol. Sci.* **28** (suppl. 2), S89–S93 (2007).
40. Disa, J., Parameswaran, N., Nambi, P. & Aiyar, N. Involvement of cAMP-dependent protein kinase and pertussis toxin–sensitive G-proteins in CGRP mediated JNK activation in human neuroblastoma cell line. *Neuropeptides* **34**, 229–233 (2000).
41. Borsello, T. & Forloni, G. JNK signalling: a possible target to prevent neurodegeneration. *Curr. Pharm. Des.* **13**, 1875–1886 (2007).
42. Perrin, V. *et al.* Implication of the JNK pathway in a rat model of Huntington's disease. *Exp. Neurol.* **215**, 191–200 (2009).
43. Mehan, S., Meena, H., Sharma, D. & Sankhla, R. JNK: a stress-activated protein kinase therapeutic strategies and involvement in Alzheimer's and various neurodegenerative abnormalities. *J. Mol. Neurosci.* **43**, 376–390 (2011).
44. Young, J.E. *et al.* Polyglutamine-expanded androgen receptor truncation fragments activate a Bax-dependent apoptotic cascade mediated by DP5/Hrk. *J. Neurosci.* **29**, 1987–1997 (2009).
45. Edvinsson, L. & Goadsby, P.J. Neuropeptides in migraine and cluster headache. *Cephalalgia* **14**, 320–327 (1994).
46. Katsuno, M. *et al.* for the Japan SBMA Interventional Trial for TAP-144-SR (JASMITT) study group. Efficacy and safety of leuprorelin in patients with spinal and bulbar muscular atrophy (JASMITT study): a multicentre, randomised, double-blind, placebo-controlled trial. *Lancet Neurol.* **9**, 875–884 (2010).
47. Fernández-Rhodes, L.E. *et al.* Efficacy and safety of dutasteride in patients with spinal and bulbar muscular atrophy: a randomised placebo-controlled trial. *Lancet Neurol.* **10**, 140–147 (2011).

ONLINE METHODS

Generation, maintenance and treatment of transgenic mice. We generated AR-24Q and AR-97Q male mice as previously described[11,48]. We used AR-97Q (Line #7-8) male mice because they show progressive muscular atrophy and weakness as well as SBMA-like pathology[25,49]. In the appropriate experiments, we administered naratriptan hydrochloride in drinking water (CAS No. 143388-64-1, Toronto Research Chemicals) to mice at a concentration of 1.8 or 18 μM in distilled water from 5 weeks of age until the end of the analysis, as described previously[14]. We performed castration or sham operations on male AR-97Q mice at the age of 5 weeks, as described previously[11,17]. We generated *Calca*-knockout mice (genetic background: 129/Sv × C57BL/6, backcrossed to C57BL/6) as previously described[50] and crossed them with the AR-97Q mice (genetic background: C57BL/6). We also used the littermates for phenotypic analyses. We used only males in this study. Background strain analyses using 96 genome-wide microsatellite markers (Aoba Genetics) demonstrated that the percentage of C57BL/6 was 99.2 ± 0.7% in the *Calca*-knockout mice used in this study. We performed all the animal experiments in accordance with the US National Institutes of Health Guide for the Care and Use of Laboratory Animals and under the approval of the Nagoya University Animal Experiment Committee.

Microarray analysis of mouse spinal cord. We analyzed alterations in gene expression using a GeneChip Mouse Genome 430 2.0 Array (Affymetrix) in male AR-97Q mice because they show a progressive motor dysfunction, muscle weakness and wasting, and they show histopathological evidence of the abnormal accumulation of the pathogenic AR within the nucleus of motor neurons, as is seen in patients with SBMA[22]. For each group (wild-type, AR-24Q and AR-97Q), we examined the male mice at 7–9, 10–12 and 13–15 weeks of age. We chose these stages because the AR-97Q mice are generally asymptomatic at 7–9 weeks of age (before-onset stage), present with mild motor impairment at 10–12 weeks (early stage) and are severely weakened with profound muscle atrophy at 13–15 weeks (advanced stage). RNA from the total spinal cord, excluding the dorsal root ganglia, was isolated from three mice of each genotype at each stage using Trizol reagent (Invitrogen) according to the manufacturer's specifications. The RNA samples were purified over RNeasy columns (Qiagen). TAKARA BIO performed the cDNA preparation, hybridization process and microarray data analysis (GEO accession GSE39865). The probe sets were extracted by the present detection call. We normalized the signals by the trimmed mean method and identified significantly different probe sets ($P < 0.005$) among the strains of mice and stages with a two-way repeated ANOVA. The criterion used to detect the differences in gene expression was a 1.5-fold change.

Assessment of motor ability. We assessed rotarod performance weekly using an Economex Rotarod (Ugo Basile) as described previously[51]. To measure grip strength, the same examiner (M.M.) placed the mice on wire netting with a Grip Strength Meter (MK-380M, Muromachikikai) and pulled them. We performed three trials weekly and recorded the best performance of the grasping power for each mouse with the examiner blinded with respect to the genotype and treatments.

Retrograde FluoroGold neurotracer labeling. We anesthetized the mice with pentobarbital and made a small incision in the skin of the left calf to expose the gastrocnemius muscle. We injected a total volume of 4.5 μl of 2.5% FluoroGold solution (Biotium) in PBS into three different parts of the muscle (proximal, middle and distal) using a 10-μl Hamilton syringe. We removed spinal cords 44 h after FluoroGold administration and post-fixed them with 4% paraformaldehyde in phosphate buffer. We counted the total number of FluoroGold-labeled motor neurons in serial 30-μm spinal cord sections with an Axio Imager M1 (Carl Zeiss).

Hematological analyses of the AR-97Q mice. We collected the blood from the mice at the advanced stage (13–15 weeks) during the dissection performed for the immunohistochemistry and immunoblotting. We measured the ALT and creatinine levels in the serum of the treated mice with the Japan Society of Clinical Chemistry standardization method (MDH-UV method) and the enzymatic method of Mitsubishi Chemical Medicine, respectively.

Plasmids, cell culture and transfection. We isolated SH-SY5Y (American Type Culture Collection No. CRL-2266) mRNA with the RNeasy Mini Kit (Qiagen) and reverse transcribed to yield cDNA. We amplified human *CALCA* cDNA from the SH-SY5Y cDNA with the PrimeStar HS DNA polymerase (Takara Bio) and Takara PCR Thermal Cycler Dice (Takara Bio). We used the following primers: 5′-AGAGGTGTCATGGGCTTCCA-3′ and 5′-GTT GGCATTCTGGGGCATGC-3′. We determined the sequence of the amplified cDNA with a CEQ8000 device (Beckman Coulter). We then cloned the human *CALCA* cDNA into pcDNA3.1/V5-His-TOPO (Invitrogen). For the promoter assay, we transfected GoClone and the pGL4 Luciferase Reporter Vector encoding the *CALCA* promoter (SwitchGear Genomics) into SH-SY5Y cells stably expressing human AR-97Q with Lipofectamine 2000 (Invitrogen). We used the Steady-Glo Luciferase Assay System (Promega) for the measurement of expression with POWERSCAN 4 (DS Pharma Biomedical). The *CALCA* promoter genomic coordinates were chr11-: 14950336–14951268. We plated the wild-type SH-SY5Y cells and those stably expressing the human AR-24Q or AR-97Q and maintained them in DMEM/F12 medium containing 10% FBS with penicillin and streptomycin. We transfected the cells in each dish with the CGRP1 or mock vector using OPTI-MEM (Invitrogen) and Lipofectamine 2000 (Invitrogen) and then differentiated them in DMEM/F12 supplemented with 20 μM retinoic acid and 1 nM 5α-dihydrotestosterone. We added FCS (5%) to the medium for the cell viability assay, but no serum was used for the cell toxicity assay because of the properties of the LDH measurement. We transfected the cells with the CGRP1 vector on days 0 and 2 for the cell viability assay and on day 0 for the LDH assay. We performed both evaluations on day 4. We selected the CGRP1-transfected SH-SY5Y cells for immunoblotting by adding 500 μg ml^{-1} of the antibiotic G418 (Sigma-Aldrich) to the medium 2 d after transfection because of the low transfection efficiency of the cells. We used nontransfected SH-SY5Y cells as selection controls. By 2 weeks after the addition of G418, the control SH-SY5Y cells had died, and we extracted the protein from the surviving CGRP1-transfected SH-SY5Y cells. We isolated human truncated AR cDNAs containing 24 or 97 CAGs (1–645 bp and 1–864 bp, respectively) from pCR3.1-full-length AR-24Q or AR-97Q vector[49] and subcloned them into the pLenti6.3/V5-DEST vector (Invitrogen), of which V5 tag was switched with EmGFP isolated from pcDNA6.2/C-EmGFP-DEST vector (Invitrogen). We transfected 293FT cells (Invitrogen) with the lentivirus vectors using the Virapower lentiviral system (Invitrogen).

SiRNA. We transfected the SH-SY5Y cells stably expressing AR-97Q with the siRNA oligonucleotide duplex at a concentration of 10 nM using Lipofectamine RNAiMAX (Invitrogen), according to the manufacturer's instructions. For knockdown of *CALCA*, we used the following oligonucleotide siRNA duplexes (Takara Bio) to transfect the SH-SY5Y AR-97Q stable cell line: against *CALCA*, sense sequence GUAAUCUGAGUACUUGCA UTT, antisense sequence AUGCAAGUACUCAGAUUACTT; control, sense sequence UCUUAAUCGCGUAUAAGGCTT, antisense sequence GCCUUAUACGCGAUUAAGATT. For knock-down of *DUSP1*, we used the following oligonucleotide siRNA duplexes (Stealth RNAi) to transfect the SH-SY5Y AR-97Q stable cell line: against *DUSP1* (1), sense sequence GACA UGCUGGAUGCCUUGGGCAUAA, antisense sequence UUAUGCCCAAG GCAUCCAGCAUGUC; against *DUSP1* (2), sense sequence GCCAUUGAC UUCAUAGACUCCAUCA, antisense sequence UGAUGGAGUCUAUGAA GUCAAUGGC. We used Stealth RNAi negative control duplex (Invitrogen) as the control for *DSUP1* siRNA.

Primary motor neuron culture. We dissected the spinal cord from C57BL/6 mouse embryos at E13. After removing meninges, dorsal root ganglia and the dorsal half of the spinal cord, we dissociated ventral part tissue into a single-cell suspension by Sumilon dissociation solution (Sumitomo Bakelite). We plated the cells at a density of 2×10^5 cells in a 24-well culture plate with Sumilon nerve-culture medium (Sumitomo Bakelite). On day 4, we infected the neurons with 3×10^5 copies μl^{-1} of lentivirus expressing truncated human AR with 24Q or 97Q[17]. After 3 h of infection, we removed the virus medium. We then cultured the neurons for 3 additional days and harvested them on day 7 followed by RNA extraction, cDNA synthesis, protein extraction, viability assay and immunocytochemistry.

Cell viability and toxicity assays. We performed the cell viability and LDH assays using WST-1 (Roche Diagnostics, Mannheim) and the Cytotoxicity Detection Kit PLUS (Roche Diagnostics), according to the manufacturer's instructions. We determined the number of dead cells using a Countess cell counter (Invitrogen) after staining with Trypan blue. We cultured the cells in 24-well plates. After each treatment, we incubated the cells with the WST-1 substrate for 3–4 h and spectrophotometrically assayed them at 440 nm using a plate reader (Powerscan HT, Dainippon Pharmaceutical). For the toxicity assays, we plated the wild-type SH-SY5Y cells and those stably expressing AR-97Q in the same medium used before transfection. The next day, we differentiated the cells in DMEM/F12 with the same supplement used after transfection. We administered the CGRP1 peptide and the CGRP1 antagonist, CGRP-1 8–37 (Peptide Institute), to the wild-type SH-SY5Y cells and those stably expressing AR-97Q in a serum-free medium for 3 d after differentiation. Two hours after treatment, we performed the cell viability assay. We also administered naratriptan hydrochloride (CAS No. 143388-64-1, Toronto Research Chemicals), rizatriptan benzoate (CAS No. 145202-66-0, Toronto Research Chemicals), sumatriptan succinate (CAS No. 103628-48-4, LKT Laboratories), SP-600125 (Merck), DUSP1 inhibitor (1 μM, Ro-31-8220, Calbiochem) and 5-HT inhibitor methiothepin mesylate (1 μM, sc-253005) in serum-free medium 3 d after differentiation. We administered naratriptan and other triptans at a concentration of 10 μM, unless otherwise mentioned. We performed the cell viability and cytotoxicity assays 24 h after drug administration.

Immunohistochemistry. We deeply anesthetized the mice and removed the entire spinal cord and skeletal muscles. We embedded the mouse samples and the autopsy specimens of the human lumbar spinal cord in paraffin[17] and performed immunohistochemistry and H&E staining as described previously[47,52]. We photographed the immunohistochemical sections with an optical microscope (Axio Imager M1, Carl Zeiss AG, Göttingen, Germany). For blocking/competition, we combined antibody (sc-8856, Santa Cruz, 1:50) with a fivefold (by weight) excess of blocking peptide (Peptide Institute). We obtained the autopsy specimens of the lumbar spinal cord from genetically diagnosed subjects with SBMA (52- and 77-year-old males) and from neurologically normal subjects (53- and 75-year-old males). The Ethics Committee of Nagoya University Graduate School of Medicine approved the collection of human tissues and their use in this study, and we obtained the written informed consent from the subjects' next of kin. We prepared 6-μm-thick sections from paraffin-embedded tissues and used the following primary antibodies: CGRP1 (sc-8856, Santa Cruz, 1:50); p-c-Jun (2361, Cell Signaling Technology, 1:100); c-Jun (#9165, Cell Signaling Technology, 1:400); GFAP (#2301-1, Epitomics, 1:250); and choline acetyltransferase (ab68779, Abcam, 1:1,000). Primary antibody binding was probed with a secondary antibody labeled with a polymer as part of the Envision+ system containing horseradish peroxidase (Dako). We measured the immunoreactivity of CGRP1 in the spinal motor neurons of SBMA and control subjects within five nonconsecutive sections with an interval of 30 μm from three subjects of each group. For the purposes of counting, we defined a motor neuron by its presence within the anterior horn and the obvious nucleolus in a given 6-μm-thick section. We calculated the intensities by multiplying the staining concentration by cell sizes using WinROOF (Mitani). We measured the immunoreactivity of p-c-Jun in more than 20 neurons within three nonconsecutive sections from each mouse ($n = 6$). For the purposes of counting, we defined a motor neuron as described above. We quantified the intensities and cell sizes with WinROOF. The means ± s.e.m. were expressed in arbitrary units.

Immunocytochemistry. We fixed mouse primary motor neurons with 4% paraformaldehyde, treated with 5% Triton X-100 and incubated them with the following primary antibodies: neurofilament H (SMI32, Covance, 1:500), GFP (598 or M048-3, MBL, 1:500) and p-c-Jun (2361, Cell Signaling Technology, 1:500).

Immunoblotting. We deeply anesthetized the mice with pentobarbital anesthesia, dissected the tissues (whole brains, spinal cords, brainstems and skeletal muscles), snap-froze them with powdered CO_2 in acetone and homogenized them in PhosphoSafe Extraction Reagent (Merck Chemicals) containing phosphatase inhibitor and HALT, which is a protease inhibitor cocktail (Thermo Scientific). We lysed the cultured cells in the same reagent after intervention. We used NE-PER Nuclear Cytoplasmic Reagents (Thermo Scientific) for the analysis of the NF-κB pathway. We separated the samples on 5–20% SDS-PAGE gels and then transferred them to Hybond-P membranes (GE Healthcare) using 25 mM Tris, 192 mM glycine, 0.1% SDS and 10% methanol as the transfer buffer. We diluted the primary and secondary antibodies with Can Get Signal, which is a signal enhancer solution (NKB-101, Toyobo). We digitized the immunoblots with an LAS-3000 imaging system (Fujifilm), quantified the signal intensities of the independent blots with Image Gauge software, version 4.22 (Fujifilm), and expressed the means ± s.e.m. in arbitrary units. We used the following primary antibodies: p-c-Jun (#2361, Cell Signaling Technology, 1:1,000); c-Jun (ab16777, Abcam, 1:40); p-JNK (NB110-66666, Novus Biologicals, 1:1,000); JNK (#9252, Cell Signaling Technology, 1:1,000); choline acetyltransferase (ab68779, Abcam, 1:1,000); DUSP1 (sc-1199, Santa Cruz, 1:100); p-NFKBIA (#9241, Cell Signaling Technology, 1:1,000); NFKBIA (#1130-1, Epitomics, 1:10,000); NF-κB p65 (sc-8008, Santa Cruz, 1:200); NF-κB p50 (sc-8414, Santa Cruz, 1:200); histone H1 (sc-8030, Santa Cruz, 1:100); α-tubulin (T5168, Sigma-Aldrich, 1:5000); phospho-ERK1/2 (4370, Cell Signaling Technology, 1:2,000); and ERK1/2 (#4695, Cell Signaling Technology, 1:1,000). We probed the primary antibody binding using horseradish peroxidase–conjugated secondary antibodies (GE Healthcare) at a dilution of 1:5,000, and detected the bands using the ECL Plus kit (GE Healthcare).

Quantitative real-time PCR. We determined the mRNA levels of the examined genes by real-time PCR as described previously[15,52]. Briefly, we extracted total RNA from the mouse spinal cords using TRIzol Reagent (Invitrogen) and from the cells using the RNeasy Mini Kit (Qiagen). We then reverse transcribed the extracted RNA into first-strand cDNA using SuperScript III reverse transcriptase (Invitrogen). We performed real-time PCR in a total volume of 50 μl that contained 25 μl 2× QuantiTect SYBR Green PCR Master Mix and 0.4 μM of each primer (Qiagen), and we detected the amplified products by the iCycler system (Bio-Rad Laboratories). The reaction conditions were 95 °C for 15 min, followed by 45 cycles of 15 s at 95 °C, 30 s at 55 °C and 30 s at 72 °C. As an internal control, we simultaneously quantified the expression level of glyceraldehyde-3-phosphate dehydrogenase (*GAPDH*). We used the following primers: 5′-GAAGAAGAAGTTCGCCTGCT-3′ and 5′-GATTCCCACACCGCTTAGAT-3′ for mouse *Calca*, 5′-CCTGGAGAAACCTGCCAAGTAT-3′ and 5′-TGAAGTCGCAGGAGACAACCT-3′ for mouse *Gapdh*, 5′-ACTGGTGCAGGACTATGTGC-3′ and 5′-CTTGTTGAAGTCCTGCGTGT-3′ for human *CALCA*, and 5′-AGCCTCAAGATCATCAGCAAT-3′ and 5′-GGACTGTGGTCATGAGTCCTT-3′ for human *GAPDH*. The weight of the gene contained in each sample was equal to the log of the starting quantity, and the standardized expression level of each mouse was equal to the weight ratio of each gene to that of *Gapdh*. We repeated the PCRs three times for each of the indicated numbers of samples.

ELISA. We extracted the lysates of the SH-SY5Y cells stably expressing AR-24Q and AR-97Q with CelLytic-M (Sigma-Aldrich) after each intervention. We used the CGRP EIA kit (Phoenix Pharmaceuticals), and corrected the loading dose with a PathScan Total α-Tubulin Sandwitch Elisa Kit (Cell Signaling Technology).

Statistical analyses. We analyzed the data using the Kaplan-Meier and log-rank tests for the survival rate, the unpaired *t*-test for two-group comparisons, and ANOVA with Dunnett's or Tukey's *post hoc* tests for multiple comparisons. We performed the statistical analyses using Statview software version 5 (HULINKS) and Prism version 4 (GraphPad Software).

48. Niwa, H., Yamamura, K. & Miyazaki, J. Efficient selection for high-expression transfectants with a novel eukaryotic vector. *Gene* **108**, 193–199 (1991).
49. Waza, M. *et al.* 17-AAG, an Hsp90 inhibitor, ameliorates polyglutamine-mediated motor neuron degeneration. *Nat. Med.* **11**, 1088–1095 (2005).
50. Oh-hashi, Y. *et al.* Elevated sympathetic nervous activity in mice deficient in alphaCGRP. *Circ. Res.* **89**, 983–990 (2001).
51. Adachi, H. *et al.* CHIP overexpression reduces mutant androgen receptor protein and ameliorates phenotypes of the spinal and bulbar muscular atrophy transgenic mouse model. *J. Neurosci.* **27**, 5115–5126 (2007).
52. Tokui, K. *et al.* 17-DMAG ameliorates polyglutamine-mediated motor neuron degeneration through well-preserved proteasome function in an SBMA model mouse. *Hum. Mol. Genet.* **18**, 898–910 (2009).

nature medicine

Viral delivery of miR-196a ameliorates the SBMA phenotype via the silencing of CELF2

Yu Miyazaki[1], Hiroaki Adachi[1], Masahisa Katsuno[1], Makoto Minamiyama[1], Yue-Mei Jiang[1], Zhe Huang[1], Hideki Doi[1], Shinjiro Matsumoto[1], Naohide Kondo[1], Madoka Iida[1], Genki Tohnai[1], Fumiaki Tanaka[1], Shin-ichi Muramatsu[2] & Gen Sobue[1]

Spinal and bulbar muscular atrophy (SBMA) is an inherited neurodegenerative disorder caused by the expansion of the polyglutamine (polyQ) tract of the androgen receptor (AR-polyQ)[1,2]. Characteristics of SBMA include proximal muscular atrophy, weakness, contraction fasciculation and bulbar involvement[3]. MicroRNAs (miRNAs) are a diverse class of highly conserved small RNA molecules that function as crucial regulators of gene expression in animals and plants[4]. Recent functional studies have shown the potent activity of specific miRNAs as disease modifiers both *in vitro* and *in vivo*[5–8]. Thus, potential therapeutic approaches that target the miRNA processing pathway have recently attracted attention[9,10]. Here we describe a novel therapeutic approach using the adeno-associated virus (AAV) vector–mediated delivery of a specific miRNA for SBMA. We found that miR-196a enhanced the decay of the AR mRNA by silencing CUGBP, Elav-like family member 2 (CELF2). CELF2 directly acted on AR mRNA and enhanced the stability of AR mRNA. Furthermore, we found that the early intervention of miR-196a delivered by an AAV vector ameliorated the SBMA phenotypes in a mouse model. Our results establish the proof of principle that disease-specific miRNA delivery could be useful in neurodegenerative diseases.

A mouse model of SBMA has been developed[11], and several therapeutic approaches for SBMA have been presented using this mouse model[11–15]. Among these approaches, the reduction of mutant AR protein levels in male mice ameliorated disease manifestations, suggesting a potential therapy for SBMA. miRNAs guide the RNA-induced silencing complex to mRNAs that have a target sequence complementary to that of the miRNA. The interaction between the miRNA and the target can occur with an incomplete complementary sequence; thus, a single miRNA can modulate complex physiological functions or disease phenotypes by regulating widespread networks[16]. Over the last several years, an important role of miRNAs in the pathogenesis of neurodegenerative disorders has been reported[5–8,17,18].

In this study, we used a miRNA microarray analysis to compare the miRNA expression in the spinal cords of male transgenic SBMA model mice expressing full-length human AR with 97 glutamine residues (AR-97Q) and in male mice expressing wild-type human AR (AR-24Q)[11]. Of more than 500 miRNAs tested, miR-196a (accession number MIMAT_0000518), miR-196b (accession number MIMAT_0001081), miR-496 (accession number MIMAT_0003738), miR miR-323-3p (accession number MIMAT_0000551) and miR-29b* (accession number MIMAT_0004523) showed a greater than two-fold upregulation in the spinal cord of AR-97Q mice at an advanced disease stage relative to the AR-24Q mice (**Fig. 1a**).

To examine the effects of these five miRNAs on the expression levels of AR mRNA transcribed from the *AR* gene, we co-transfected synthetic miRNAs with vectors expressing human AR-24Q or AR-97Q into HEK293T cells. Among these five miRNAs, miR-196a and miR-196b downregulated the AR mRNA and protein (**Fig. 1b,c**), although the transgene used in both the *in vitro* and *in vivo* experiments lacked the DNA sequence that encodes the AR mRNA 3′ untranslated region (UTR) (**Supplementary Fig. 1**). To determine whether the decrease in the AR mRNA level was due to the enhancement of mRNA degradation or a decrease in mRNA synthesis, we assessed the turnover of AR mRNA using an RNA stability assay with actinomycin D. In the absence of miR-196a and miR-196b, the AR mRNA had a half-life of >1.5 h. The AR mRNA had a half-life of <0.5 h in the presence of miR-196a and miR-196b (**Fig. 1d**). These findings indicated that miR-196a and miR-196b enhanced the degradation of AR mRNA via an interaction with cofactors that were able to stabilize both the wild-type and mutant AR mRNAs.

To elucidate the molecular mechanisms by which miR-196a and miR-196b regulate the stability of AR mRNA, we analyzed their potential targets using the bioinformatics program TargetScan Release 6.0. Among the hundreds of mRNAs targeted by miR-196a and miR-196b, CELF2 mRNA has a common binding site for miR-196a and miR-196b that is broadly conserved among vertebrates (**Supplementary Fig. 2**). We found that CELF2 mRNA and protein levels were significantly reduced by treatment with miR-196a and miR-196b in HEK293T cells (**Fig. 1e**) and that CELF2 was required for AR mRNA stability

[1]Department of Neurology, Nagoya University Graduate School of Medicine, Nagoya, Japan. [2]Division of Neurology, Department of Medicine, Jichi Medical University, Tochigi, Japan. Correspondence should be addressed to G.S. (sobueg@med.nagoya-u.ac.jp).

Received 3 October 2011; accepted 18 April 2012; published online 3 June 2012; doi:10.1038/nm.2791

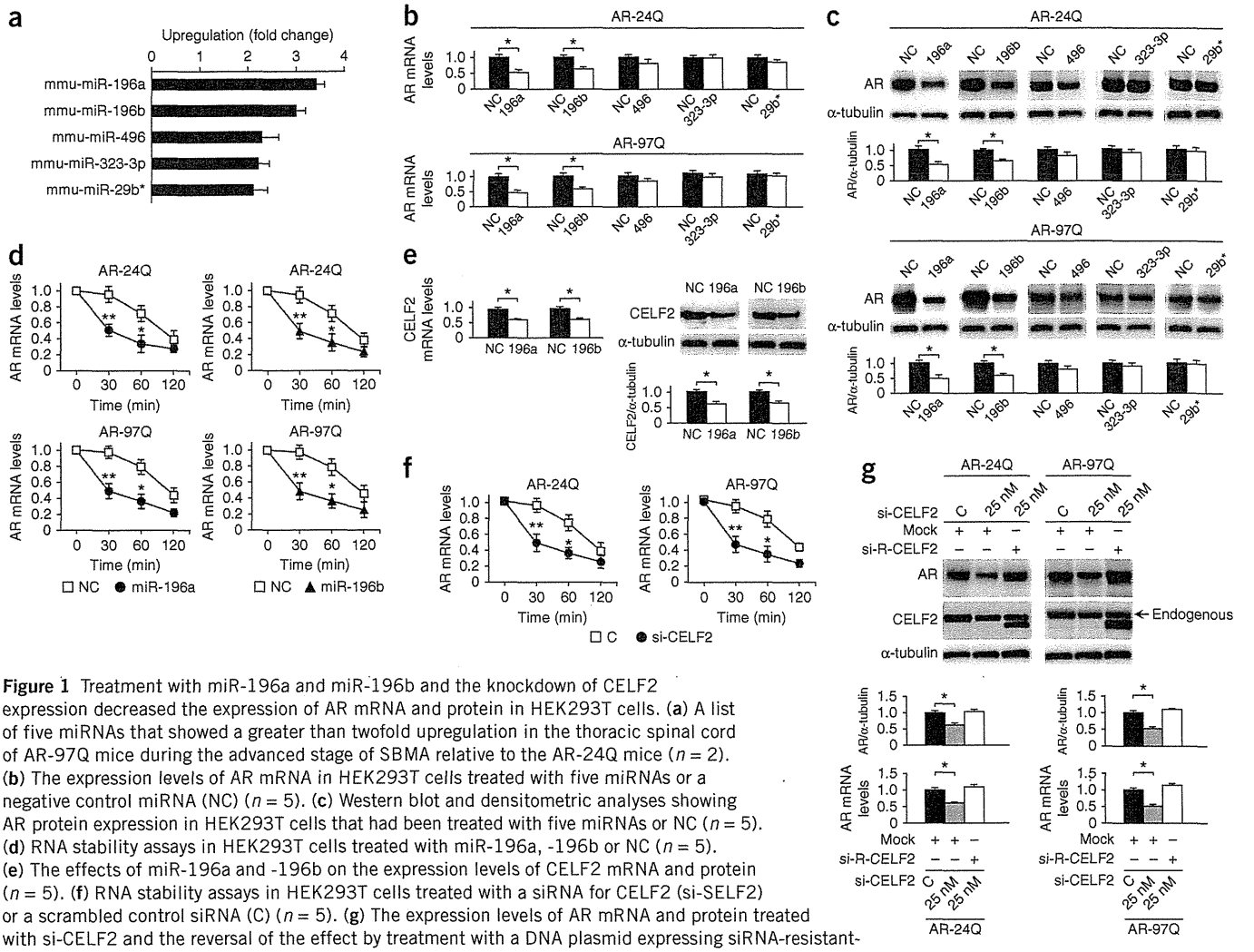

Figure 1 Treatment with miR-196a and miR-196b and the knockdown of CELF2 expression decreased the expression of AR mRNA and protein in HEK293T cells. (**a**) A list of five miRNAs that showed a greater than twofold upregulation in the thoracic spinal cord of AR-97Q mice during the advanced stage of SBMA relative to the AR-24Q mice ($n = 2$). (**b**) The expression levels of AR mRNA in HEK293T cells treated with five miRNAs or a negative control miRNA (NC) ($n = 5$). (**c**) Western blot and densitometric analyses showing AR protein expression in HEK293T cells that had been treated with five miRNAs or NC ($n = 5$). (**d**) RNA stability assays in HEK293T cells treated with miR-196a, -196b or NC ($n = 5$). (**e**) The effects of miR-196a and -196b on the expression levels of CELF2 mRNA and protein ($n = 5$). (**f**) RNA stability assays in HEK293T cells treated with a siRNA for CELF2 (si-SELF2) or a scrambled control siRNA (C) ($n = 5$). (**g**) The expression levels of AR mRNA and protein treated with si-CELF2 and the reversal of the effect by treatment with a DNA plasmid expressing siRNA-resistant-CELF2 (si-R-CELF2) ($n = 5$). All data are means ± s.e.m. $^*P < 0.05$ and $^{**}P < 0.01$. We analyzed the results by unpaired *t* tests in **b**, **c** and **e**; by two-way ANOVA followed by the Bonferroni test comparing HEK293T cells treated with miR-196a or miR-196b to cells treated with NC in **d**; by two-way ANOVA followed by the Bonferroni test comparing HEK293T cells treated with si-CELF2 to cells treated with control siRNA in **f**; and by the Dunnett test in **g**.

(**Fig. 1f**). The knockdown of CELF2 expression with specific small interfering RNAs (siRNAs) silenced CELF2 protein, accelerated the degradation of AR mRNA and led to a decrease in AR protein expression levels (**Fig. 1g**). These downregulating effects were reversed in rescue experiments using a DNA plasmid that expressed siRNA-resistant CELF2, thus confirming the interaction between CELF2 and AR mRNA (**Fig. 1g**). In contrast to the knockdown and rescue results, the overexpression of CELF2 increased the expression levels of AR mRNA and protein (**Fig. 2a**) and increased the stability of the AR mRNA (**Fig. 2b**). To determine the region of the AR mRNA that interacts with CELF2, we prepared several constructs of the mutated *AR* transgene that lacked the CAG repeats (AR-0Q) or the three triplet repeats of the CUGCUGCUG sequence (ΔCUG-AR-24Q and ΔCUG-AR-97Q), which is immediately proximal to the CAG repeats in exon 1 of the AR mRNA and is conserved in the endogenous human AR mRNA (**Fig. 2c**). Although the overexpression of CELF2 increased the expression levels of AR mRNA and protein transcribed from the mutated transgene lacking CAG repeats, the expression levels of AR mRNA and protein transcribed from the mutated transgene lacking the three triplet repeats of the CUGCUGCUG sequence were not increased relative to controls by CELF2 (**Fig. 2d**). In addition, immunoprecipitation-coupled quantitative real time-PCR (qRT-PCR) revealed the binding affinity of CELF2 to the three triplet repeats of the CUGCUGCUG sequence in exon 1 of the AR mRNA (**Fig. 2e**). On the basis of these findings, we concluded that miR-196a and miR-196b were able to decrease the expression levels of AR mRNA and protein by silencing CELF2, a protein that enhances the stability of AR mRNA through direct binding to the CUG triplet repeat sequence in exon 1 of the AR mRNA.

To examine the effects of CELF2 silencing on the motor impairment of SBMA mice, we constructed an *in vivo* delivery system based on an AAV vector that allowed for the simultaneous expression of enhanced green fluorescent protein (EGFP) and either miR-196a (AAV-miR-196a) or a nonspecific miRNA, miR-mock (AAV-miR-mock). We chose to use miR-196a instead of miR-196b because the expression of miR-196a was highly upregulated in the cytoplasm of the motor neurons of AR-97Q mice (**Supplementary Fig. 3**). A viral load of 10^{11} vector genomes (vg) of each of these constructs was injected into the skeletal muscle of the left quadriceps femoris of AR-97Q mice. The AAV vector can be transported efficiently in a retrograde manner from muscle to the motor neurons of the spinal cord[19,20] and can spread hematogenously[21,22]. Two weeks after AAV vector injection,

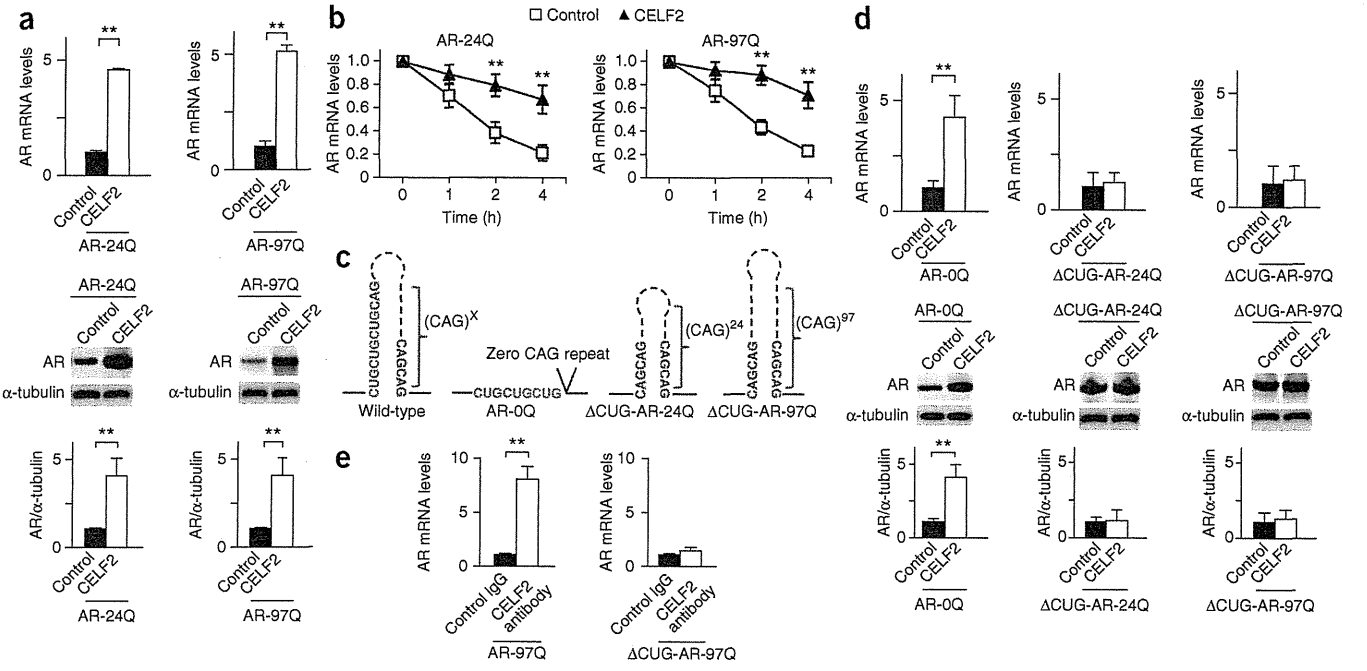

Figure 2 CELF2 recognizes the sequence CUGCUGCUG in exon 1 of the AR mRNA and increases the stability of the AR mRNA. (**a**) The expression levels of AR mRNA and protein in HEK293T cells treated with the DNA plasmid expressing human CELF2 (CELF2) or the original pcDNA3.1/HisC vector (control) ($n = 5$). (**b**) RNA stability assays in HEK293T cells treated with CELF2 or control ($n = 5$). (**c**) Schematic diagrams of the AR mRNA structure near the hairpin loop of the CAG repeats (red) transcribed from wild-type and mutated DNA plasmids. AR-0Q lacks the CAG repeats, and ΔCUG-AR-24Q and ΔCUG-AR-97Q lack the sequence CUGCUGCUG (blue) immediately adjacent to the CAG repeats. (**d**) AR mRNA and protein expression levels in HEK293T cells co-transfected with CELF2 and the mutated DNA plasmids expressing AR ($n = 5$). (**e**) The amount of AR-97Q and ΔCUG-AR-97Q mRNA binding to CELF2 that was immunoprecipitated using an antibody against CELF2 or a control immunoglobulin (IgG) ($n = 5$). All data are means ± s.e.m. $^{**}P < 0.01$ (we analyzed the results by unpaired *t* tests in **a**,**d** and **e** and by two-way ANOVA followed by the Bonferroni test comparing HEK293T cells treated with CELF2 to cells treated with control in **b**).

a widespread transduction of the viral particles throughout the brain, spinal cord and the skeletal muscle of the upper and lower limbs was observed (**Supplementary Fig. 4a**). There was no difference in the expression of EGFP between the left and right sides of the spinal cord (**Supplementary Fig. 4b**). The presence of the AAV vector in the motor neurons of infected mice was visually confirmed by the colocalization of EGFP and staining for choline acetyltransferase (ChAT), a motor neuron marker (**Supplementary Fig. 4c**). Because the widespread viral transduction throughout the entire body was also detected in mice in which virus was injected into a cardiac chamber (**Supplementary Fig. 4d**), we deduced that the viral particles injected into the hind limb skeletal muscle spread hematogenously throughout the entire body of the mouse. In addition to viral distribution, a tyrosine mutation of the adeno-associated viral capsid protein may contribute to the enhanced transgene expression levels delivered by AAV[23]. We then did an AAV vector injection into the quadriceps femoris of a 5-week-old mouse, before the onset of motor impairment in the SBMA mice (approximately 7 weeks of age), because transgene expression stabilizes approximately 2 weeks after vector delivery.

The disease progression in the AR-97Q mice treated with AAV-miR-196a (AR-97Q-miR-196a mice) was ameliorated compared with AAV-miR-mock-treated mice. The AR-97Q mice treated with AAV-miR-mock (AR-97Q-miR-mock mice) showed motor impairment, as assessed by the rotarod task, as early as 7 weeks after birth. By contrast, the AR-97Q-miR-196a mice showed an initial impairment at 13 weeks after birth but showed less deterioration than their AR-97Q-miR-mock counterparts ($P < 0.001$) (**Fig. 3a**). The locomotor cage activity of the AR-97Q-miR-mock mice was also markedly decreased at 7 weeks compared with that of the AR-97Q-miR-196a mice ($P < 0.001$), which showed decreased activity at 13 weeks of age (**Fig. 3b**). Moreover, the AR-97Q-miR-mock mice lost weight significantly earlier and more profoundly than the AR-97Q-miR-196a mice ($P < 0.001$) (**Fig. 3c**). Treatment with miR-196a significantly prolonged the survival of the AR-97Q-miR-196a mice ($P < 0.001$) compared with the AR-97Q-miR-mock mice (**Fig. 3d**). By 12 weeks of age, the AR-97Q-miR-mock mice showed obvious differences in body size, muscular atrophy and kyphosis compared with the AR-97Q-miR-196a mice (**Fig. 3e**). In addition, the AR-97Q-miR-mock mice showed motor weakness, as indicated by short steps and leg dragging, whereas the AR-97Q-miR-196a mice showed almost normal ambulation (**Fig. 3f**). Immunohistochemical examination of mouse tissues using 1C2 antibody, which specifically recognizes the expanded polyQ region in the mutant AR, showed a marked reduction in 1C2-positive nuclear accumulation in the anterior horn of the thoracic spinal cord and in the skeletal muscles of the right quadriceps femoris of the AR-97Q-miR-196a mice compared with those of the AR-97Q-miR-mock mice. Glial fibrillary acidic protein (GFAP)-specific antibody staining showed that the AAV vector–mediated delivery of miR-196a reduced reactive astrogliosis in the thoracic spinal anterior horn of the AR-97Q mice, thereby suggesting that miR-196a attenuated neurodegenerative changes. Histopathological examination of the skeletal muscle showed marked amelioration of neurogenic muscle atrophy in the AR-97Q-miR-196a mice compared with the AR-97Q-miR-mock mice (**Fig. 3g**). By quantitative assessment, we confirmed that AAV-miR-196a significantly reduced 1C2-positive nuclear accumulation in the anterior horn of the thoracic spinal cord ($P < 0.01$) and

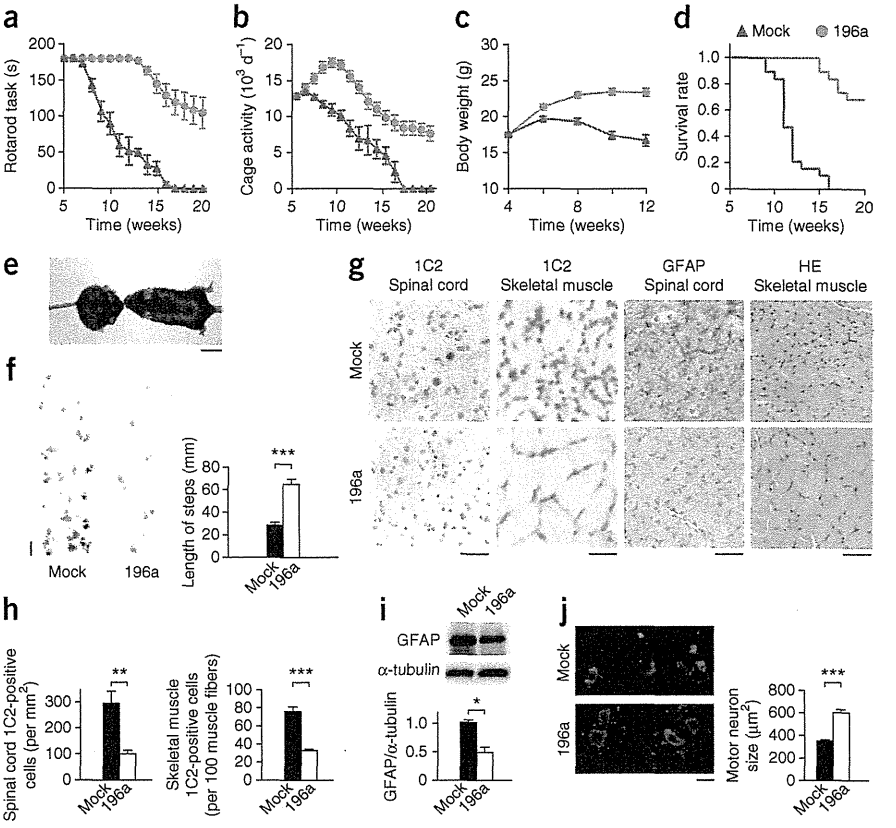

Figure 3 The effects of miR-196a on the phenotype of male AR-97Q mice. (**a–d**) A rotarod task (**a**), cage activity (**b**), body weight (**c**) and survival rate (Kaplan-Meier analysis and log-rank test) (**d**) of the AR-97Q-miR-mock (mock) or AR-97Q-miR-196a mice (196a) ($n = 19$ in each group). $P < 0.001$ for all data at each time after 8 weeks of age in **a–c**. (**e**,**f**) A representative photograph (**e**) and footprints (**f**) of a 12-week-old AR-97Q-miR-mock mouse (left) and an age-matched AR-97Q-miR-196a mouse (right). The front and hind paws are indicated in red and blue, respectively. Each column shows the average length of the steps taken by the hind paw ($n = 5$). Scale bars, 20 mm. (**g**) Immunohistochemical staining for the mutant AR using the 1C2 antibody of the thoracic spinal cord and skeletal muscle of the right quadriceps femoris; immunohistochemical staining with a GFAP-specific antibody of the thoracic spinal anterior horn; and hematoxylin and eosin (HE) staining of the skeletal muscle of the right quadriceps femoris. Scale bars, left to right: 50 μm, 10 μm, 50 μm, 20 μm. (**h**) Quantification of 1C2-positive cells in the thoracic spinal cord and skeletal muscle of the right quadriceps femoris ($n = 5$). (**i**) Western blot and densitometric analyses showing the levels of GFAP protein expression in the thoracic spinal cord ($n = 5$). (**j**) The mean size of the motor neurons of the thoracic spinal cord obtained from AR-97Q-miR-196a mice compared with that of AR-97Q-miR-mock mice ($n = 5$). Scale bar, 20 μm. All data are means ± s.e.m. $^*P < 0.05$, $^{**}P < 0.01$ and $^{***}P < 0.001$ (we analyzed the results by two-way ANOVA followed by the Bonferroni test comparing the mock to 196a in **a–c** and by unpaired t test in **f**, **h–j**).

in the skeletal muscle of the right quadriceps femoris ($P < 0.001$) of the AR-97Q-mice (**Fig. 3h**). Western blot analyses and quantification of the immunohistochemical signal intensities revealed that treatment with miR-196a downregulated the expression levels of GFAP (**Fig. 3i** and **Supplementary Fig. 5**). In addition, treatment with miR-196a significantly suppressed motor neuron shrinkage ($P < 0.001$) (**Fig. 3j**).

At 3 weeks after injection of a viral load of 10^{11} vg, we killed the mice and harvested the RNA and protein in the thoracic spinal cord for analysis. The AR-97Q-miR-196a mice showed high expression levels of miR-196a and low expression levels of CELF2 mRNA, mutant AR mRNA and the endogenous mouse AR mRNA in the thoracic spinal cord compared with AR-97Q-miR-mock mice (**Fig. 4a**). The mouse AR mRNA lacks a CUGCUGCUG tract; however, it has the CUGCUG sequence in its coding region that would interact with CELF2. Western blotting analyses of thoracic spinal cord lysates of the AR-97Q-miR-mock mice showed that the high-molecular-weight mutant AR protein complex was retained in the stacking gel and that a monomeric AR migrated as a band through the separating gel (**Fig. 4b**). Treatment with AAV-miR-196a notably reduced both the high-molecular-weight complex and the monomer of AR and CELF2 in the thoracic spinal cord (**Fig. 4b**). We observed the elevated expression levels of miR-196a achieved by AAV vector–mediated expression and the decreased expression levels of mutant AR mRNA in the thoracic spinal cord throughout the follow-up period of 15 weeks (**Fig. 4c**). Although we detected the effects of the miR-196a treatment in the skeletal muscle, we found that the increase in the levels of miR-196a expression and the downregulation of mutant AR mRNA and protein were more prominent in the spinal cord than in the skeletal muscle (**Supplementary Fig. 6**). The skeletal muscle of the right quadriceps femoris, contralateral to the site of the AAV vector injection, also showed treatment effects (**Supplementary Fig. 6**). AR-97Q-miR-196a mice showed no detectable reduction in the normal serum testosterone levels, which has been shown to directly affect the levels of AR expression (**Fig. 4d**)[11].

To address whether miR-196a-mediated treatment can be useful in the therapy of patients with SBMA, we examined the effects of miR-196a on AR mRNA and protein in fibroblasts obtained from patients with SBMA and from disease control subjects. Treatment with miR-196a downregulated both the AR and CELF2 mRNAs and proteins in the fibroblasts obtained from patients with SBMA (**Fig. 4e**) and disease control subjects (**Supplementary Fig. 7**). We also observed similar effects for AR mRNA and protein in fibroblasts treated with CELF2 siRNA (**Fig. 4f**). Taken together, these findings suggest that miR-196a-mediated treatment might be useful in the therapy of patients with SBMA. Furthermore, we measured the expression levels of miR-196a, miR-196b and CELF2 mRNA in the thoracic spinal cord of patients with SBMA. Both of the two miRNAs were upregulated and the CELF2 mRNA was downregulated in the thoracic spinal cord of patients with SBMA compared with those of disease control subjects (**Fig. 4g**). qRT-PCR revealed that the expression levels of CELF2 mRNA were lower in the thoracic spinal cord of AR-97Q mice than in AR-24Q mice (**Supplementary Fig. 8**), thereby confirming the correlations between the *in vivo* levels of the two miRNAs and CELF2 mRNA. We also showed the *in vivo* correlation between miR-196a and mutant AR mRNA levels and monitored the side effects of mice treated with AAV-miR-196a (**Supplementary Note**

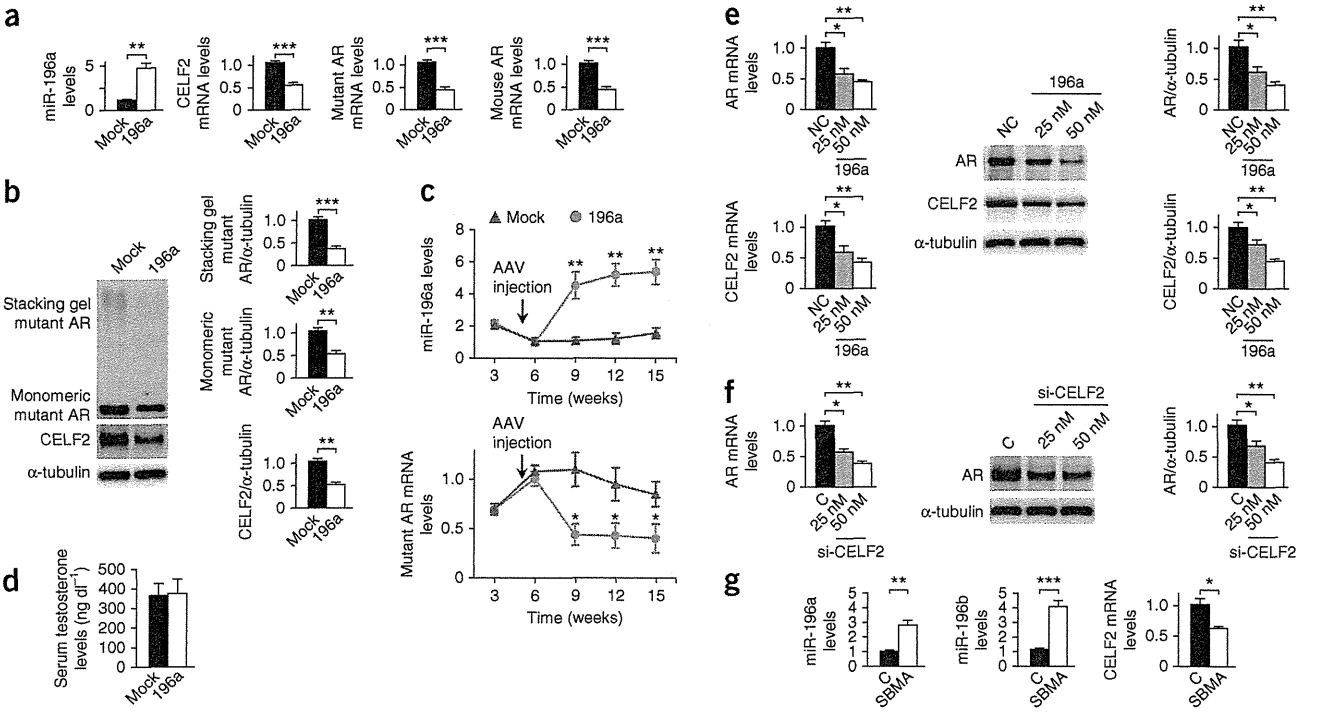

Figure 4 The effects of miR-196a on mutant AR expression in male AR-97Q mice and patients with SBMA. (**a**) The levels of miR-196a, CELF2 mRNA, mutant AR mRNA and the endogenous mouse AR mRNA expression in the thoracic spinal cord of AR-97Q-miR-mock (mock) and AR-97Q-miR-196a (196a) mice ($n = 5$). (**b**) Western blot and densitometric analyses showing the expression levels of mutant AR both in the stacking and separating gels as well as those of CELF2 ($n = 5$). (**c**) A temporal change in the levels of miR-196a and mutant AR mRNA expression in the thoracic spinal cord of AR-97Q-miR-mock and AR-97Q-miR-196a mice ($n = 3$ to 4). (**d**) The serum testosterone levels of AR-97Q-miR-mock and AR-97Q-miR-196a mice ($n = 5$). (**e**) The expression levels of mutant AR mRNA, CELF2 mRNAs and their proteins in the fibroblasts of patients with SBMA ($n = 5$). NC, a negative control miRNA. (**f**) The effects of CELF2 silencing on mutant AR mRNA and protein in the fibroblasts of patients with SBMA ($n = 5$). C, a scrambled control siRNA. (**g**) The expression levels of miR-196a, -196b and CELF2 mRNA in the thoracic spinal cord of patients with SBMA ($n = 3$). C, disease control subjects. All data are means ± s.e.m. $^*P < 0.05$, $^{**}P < 0.01$ and $^{***}P < 0.001$ (we analyzed the results by unpaired t tests in **a**,**b**,**d** and **g** and by two-way ANOVA followed by the Bonferroni test comparing the mock to 196a in **c**, and by the Dunnett test in **e**,**f**).

and **Supplementary Fig. 8**). In addition, we examined the post-translational effects of miR-196a in HEK293T and the effects of miR-196a on apoptosis in Neuro2a cells (**Supplementary Note** and **Supplementary Fig. 9**). We also showed the effects of miR-196a downregulation on mutant AR mRNA and protein in HEK293T cells (**Supplementary Note** and **Supplementary Fig. 10**).

In this study, we showed that miR-196a is upregulated in the spinal cord of a transgenic mouse model of SBMA during the symptomatic stage and that early intervention by the transduction of mice with miR-196a via an AAV vector can markedly ameliorate the motor impairment of SBMA mice. We further showed that miR-196a silences CELF2, which then directly acts on AR mRNA to affect its stability. Although polyQ models have been shown to have altered miRNA profiles[7,17] and miRNAs targeting of the polyQ disease gene have been proposed as disease modifiers [6,7], the miRNA-mediated therapeutic approach targeting a regulator of the disease transcript described in our study is conceptually novel and could be strategically applied to other polyQ-related diseases.

The upregulation of miR-196a has been reported in a wide variety of cancers[24,25] and has also been shown to be involved in differentiation[26,27] and the development of the immune system[28]. Hence, miR-196a has previously been proposed as a therapeutic target for these ailments. Similarly, the modulation of CELF2 has known implications for myotonic dystrophy[29] and several cancer types[30,31].

Our results show that the strong and continuous inhibition of the expression of CELF2 by the AAV vector–mediated delivery of miR-196a has a substantial effect on the SBMA phenotype. Although the reason for the natural upregulation of miR-196a in the spinal cord of SBMA mice and patients with SBMA is unknown, it may indicate a protective mechanism that is insufficient alone but sufficiently beneficial when amplified by AAV-mediated overexpression. However, whether similarly effective therapy would result from injections to an isolated skeletal muscle in patients with SBMA must be verified. The appropriate route and the required dose of AAV administration should be determined in future studies. Our findings indicate that the miRNA-mediated regulation of RNA metabolism is a logical target for the therapeutic intervention of SBMA and they suggest a new therapeutic approach using an AAV vector–mediated miRNA delivery system for the treatment of neurodegenerative disease.

METHODS

Methods and any associated references are available in the online version of the paper.

Note: Supplementary information is available in the online version of the paper.

ACKNOWLEDGMENTS

We are grateful to T. Cooper (Department of Pathology and Immunology, Baylor College of Medicine) for kindly providing the plasmid expressing human CELF2. We also thank N. Takino, H. Miyauchi and K. Ayabe (Division of Neurology, Department of Medicine, Jichi Medical University) for their help with the production of the AAV vectors and Y. Kondo and K. Shinjo (Division of Molecular Oncology, Aichi Cancer Center Research Institute) for expert technical support and helpful discussions. This work was supported by grants from the Ministry of Health,

Labor and Welfare; grants from the Ministry of Education, Culture, Sports, Science, and Technology of Japan; a Center-of-Excellence (COE) grant; a Grant-in-Aid for Scientific Research on Innovated Areas "Foundations of Synapse and Neurocircuit Pathology"; and the Core Research for Evolutional Science and Technology (CREST) program of the Japan Science and Technology Agency (JST).

AUTHOR CONTRIBUTIONS

Project planning was done by Y.M., H.A., M.K., F.T., S. Muramatsu and G.S.; experimental work was done by Y.M., H.A., M.K., M.M., Y.-M.J., Z.H., H.D., S. Matsumoto, N.K., M.I., G.T. and S. Muramatsu; data analysis was done by Y.M., H.A., M.K., F.T., S. Muramatsu and G.S.; the manuscript was written by Y.M., H.A., M.K., F.T., S. Muramatsu and G.S.

COMPETING FINANCIAL INTERESTS

The authors declare no competing financial interests.

Published online at http://www.nature.com/doifinder/10.1038/nm.2791.
Reprints and permissions information is available online at http://www.nature.com/reprints/index.html.

1. La Spada, A.R., Wilson, E.M., Lubahn, D.B., Harding, A.E. & Fischbeck, K.H. Androgen receptor gene mutations in X-linked spinal and bulbar muscular atrophy. *Nature* **352**, 77–79 (1991).
2. Kennedy, W.R., Alter, M. & Sung, J.H. Progressive proximal spinal and bulbar muscular atrophy of late onset: a sex-linked recessive trait. *Neurology* **50**, 583–593 (1998).
3. Sobue, G. *et al.* X-linked recessive bulbospinal neuronopathy. A clinicopathological study. *Brain* **112**, 209–232 (1989).
4. Kim, V.N., Han, J. & Siomi, M.C. Biogenesis of small RNAs in animals. *Nat. Rev. Mol. Cell Biol.* **10**, 126–139 (2009).
5. Kim, J. *et al.* A MicroRNA feedback circuit in midbrain dopamine neurons. *Science* **317**, 1220–1224 (2007).
6. Karres, J.S., Hilgers, V., Carrera, I., Treisman, J. & Cohen, S.M. The conserved microRNA miR-8 tunes atrophin levels to prevent neurodegeneration in *Drosophila*. *Cell* **131**, 136–145 (2007).
7. Lee, Y. *et al.* miR-19, miR-101 and miR-130 co-regulate ATXN1 levels to potentially modulate SCA1 pathogenesis. *Nat. Neurosci.* **11**, 1137–1139 (2008).
8. Williams, A.H. *et al.* MicroRNA-206 delays ALS progression and promotes regeneration of neuromuscular synapses in mice. *Science* **326**, 1549–1554 (2009).
9. Roshan, R., Ghosh, T., Scaria, V. & Pillai, B. MicroRNAs: novel therapeutic targets in neurodegenerative diseases. *Drug Discov. Today* **14**, 1123–1129 (2009).
10. Boudreau, R.L., Rodríguez-Lebrón, E. & Davidson, B.L. RNAi medicine for the brain: progresses and challenges. *Hum. Mol. Genet.* **20**, R21–R27 (2011).
11. Katsuno, M. *et al.* Testosterone reduction prevents phenotypic expression in a transgenic mouse model of spinal and bulbar muscular atrophy. *Neuron* **35**, 843–854 (2002).
12. Katsuno, M. *et al.* Leuprorelin rescues polyglutamine-dependent phenotypes in a transgenic mouse model of spinal and bulbar muscular atrophy. *Nat. Med.* **9**, 768–773 (2003).
13. Adachi, H. *et al.* Heat shock protein 70 chaperone overexpression ameliorates phenotypes of the spinal and bulbar muscular atrophy transgenic mouse model by reducing nuclear-localized mutant androgen receptor protein. *J. Neurosci.* **23**, 2203–2211 (2003).
14. Waza, M. *et al.* 17-AAG, an Hsp90 inhibitor, ameliorates polyglutamine-mediated motor neuron degeneration. *Nat. Med.* **11**, 1088–1095 (2005).
15. Tokui, K. *et al.* 17-DMAG ameliorates polyglutamine-mediated motor neuron degeneration through well-preserved proteasome function in an SBMA model mouse. *Hum. Mol. Genet.* **18**, 898–910 (2009).
16. Eacker, S.M., Dawson, T.M. & Dawson, V.L. Understanding microRNAs in neurodegeneration. *Nat. Rev. Neurosci.* **10**, 837–841 (2009).
17. Bilen, J., Liu, N., Burnett, B.G., Pittman, R.N. & Bonini, N.M. MicroRNA pathways modulate polyglutamine-induced neurodegeneration. *Mol. Cell* **24**, 157–163 (2006).
18. Schaefer, A. *et al.* Cerebellar neurodegeneration in the absence of microRNAs. *J. Exp. Med.* **204**, 1553–1558 (2007).
19. Kaspar, B.K. *et al.* Retrograde viral delivery of IGF-1 prolongs survival in a mouse ALS model. *Science* **301**, 839–842 (2003).
20. Towne, C. *et al.* Efficient transduction of non-human primate motor neurons after intramuscular delivery of recombinant AAV serotype 6. *Gene Ther.* **17**, 141–146 (2010).
21. Dominguez, E. *et al.* Intravenous scAAV9 delivery of a codon-optimized SMN1 sequence rescues SMA mice. *Hum. Mol. Genet.* **20**, 681–693 (2011).
22. Fu, H., Dirosario, J., Killedar, S., Zaraspe, K. & McCarty, D.M. Correction of neurological disease of mucopolysaccharidosis IIIB in adult mice by rAAV9 trans-blood-brain barrier gene delivery. *Mol. Ther.* **19**, 1025–1033 (2011).
23. Petrs-Silva, H. *et al.* Novel properties of tyrosine-mutant AAV2 vectors in the mouse retina. *Mol. Ther.* **19**, 293–301 (2011).
24. Hui, A.B. *et al.* Robust global micro-RNA profiling with formalin-fixed paraffin-embedded breast cancer tissues. *Lab. Invest.* **89**, 597–606 (2009).
25. Maru, D.M. *et al.* MicroRNA-196a is a potential marker of progression during Barrett's metaplasia-dysplasia-invasive adenocarcinoma sequence in esophagus. *Am. J. Pathol.* **174**, 1940–1948 (2009).
26. Yekta, S., Shih, I.H. & Bartel, D.P. MicroRNA-directed cleavage of HOXB8 mRNA. *Science* **304**, 594–596 (2004).
27. Hornstein, E. *et al.* The microRNA miR-196 acts upstream of Hoxb8 and Shh in limb development. *Nature* **438**, 671–674 (2005).
28. Pedersen, I.M. *et al.* Interferon modulation of cellular microRNAs as an antiviral mechanism. *Nature* **449**, 919–922 (2007).
29. Dhaenens, C.M. *et al.* Mis-splicing of *Tau* exon 10 in myotonic dystrophy type 1 is reproduced by overexpression of CELF2 but not by MBNL1 silencing. *Biochim. Biophys. Acta* **1812**, 732–742 (2011).
30. Natarajan, G. *et al.* CUGBP2 downregulation by prostaglandin E2 protects colon cancer cells from radiation-induced mitotic catastrophe. *Am. J. Physiol. Gastrointest. Liver Physiol.* **294**, G1235–G1244 (2008).
31. Subramaniam, D. *et al.* RNA binding protein CUGBP2/CELF2 mediates curcumin-induced mitotic catastrophe of pancreatic cancer cells. *PLoS ONE* **6**, e16958 (2011).

ONLINE METHODS

Construction of DNA plasmids. We constructed cDNA expression plasmids encoding full-length AR by subcloning AR cDNA derived from pSP64-AR24 and pSP64-AR97 (ref. 32) into the pCR3.1 mammalian expression vector (Life Technologies). We carried out an L55 L56 L57 (CTGCTGCTG) deletion of AR-24Q and AR-97Q as follows: the pBS+AflII plasmid was generated by the insertion of an AflII linker into the EcoRV site of pBluescript II KS(−). We excised the 417-bp fragment of 24Q and the 636-bp fragment of 97Q from pCR3.1-AR-24Q and -97Q using SmaI and AflII and cloned it into the SmaI and AflII sites of pBS+AflII to create pBS-24Q and -97Q. pBS-ΔCUG-24Q and -97Q were constructed by inserting the double-stranded oligomer CCAGTTTGCA into pBS-24Q and -97Q digested with NarI-PstI (blunted). Finally, we re-excised the pBS-ΔCUG-24Q and -97Q with SmaI-AflII and inserted this fragment between the SmaI and AflII sites of pCR3.1-AR to form pCR3.1-AR ΔCUG-24Q and -97Q.

The CAG repeat deletion of the AR construct was generated using a KOD-Plus-Mutagenesis kit (Toyobo) with the forward primer 5′-CAAGAG ACTAGCCCCAGGCAGCAGC-3′ and the reverse primer 5′-CAGCAGCA GCAAACTGGCGCCG-3′. The DNA plasmid expressing human CELF2 was kindly provided by T. Cooper (Professor, Department of Pathology and Immunology, Baylor College of Medicine). The siRNA-resistant construct was generated by changing the siRNA targeted sequence (5′- GAATGCACTGCACA ATATT -3′) of pcDNA3.1/HisC-CELF2 to 5′- AAACGCGCTACATAACATC -3′ (mutated nucleotides are underlined) using a KOD-Plus-Mutagenesis kit (Toyobo) with the forward primer 5′-ACATAACATCAAAACTTTACCTGG GATGCATCATCCCA-3′ and the reverse primer 5′-AGCGCGTTTTGGGCC TCAAGTGCAGCTTTTCTTGTATA-3′. The sequences of all mutations and the CAG repeat length were confirmed using a CEQ 8000 Genetic Analysis System (Beckman Coulter). We used the original pcDNA3.1/HisC vector lacking the insertions in the multiple cloning sites as a mock vector.

Co-transfection of DNA plasmids with either synthetic miRNA or siRNA into cultured cells. The sequences of the siRNA target for CELF2 mRNA are 5′-GAATGCACTGCACAATATT-3′ (accession number NM_001025076), 5′-CACCTATCGTGGTGAAGTT-3′ (accession number NM_001025076) and 5′- CACAGTATCTGGCGCTCCT-3′ (accession number NM_001025076). All of the siRNAs were purchased from Sigma-Aldrich. A scrambled control siRNA (MISSION siRNA Universal Negative Control SIC-001; Sigma-Aldrich), synthetic miR-196a (MISSION microRNA Mimics -hsa-miR-196a; Sigma-Aldrich), synthetic miR-196b (MISSION microRNA Mimics -hsa-miR-196b; Sigma-Aldrich), synthetic miR-496 (MISSION microRNA Mimics -hsa-miR-496; Sigma-Aldrich), synthetic miR-323-3p (MISSION microRNA Mimics -hsa-miR-323-3p; Sigma-Aldrich), synthetic miR-29b* (Syn-mmu-miR-29b-1* miScript miRNA Mimic; Qiagen), anti-miR-196a antisense (anti-hsa-miR-196a miScript miRNA Inhibitor; Qiagen) and negative control miRNA (MISSION microRNA Mimic, Human, Negative Control 1; Sigma-Aldrich) were purchased. We plated HEK293T cells onto six-well dishes and co-transfected each dish with 0.5 μg of the vector containing the following: AR-24Q, AR-97Q, ΔCUG-AR-24Q, ΔCUG-AR-97Q or AR-0Q; 2.0 μg of the vector containing CELF2, siRNA-resistant CELF2 or mock; and either 25 nM synthetic miRNA or 25 nM siRNA molecules. We used Lipofectamine 2000 (Life Technologies) as a transfection reagent in the cases in which all of the RNAi molecules purchased from Sigma-Aldrich were transfected into the HEK293T cells or Neuro2a cells. For the transfection of synthetic miR-29b* (Syn-mmu-miR-29b-1* miScript miRNA Mimic; Qiagen) and anti-miR-196a antisense (anti-hsa-miR-196a miScript miRNA Inhibitor; Qiagen) into HEK293T cells, we used the Attractene Transfection Reagent (Qiagen) as a transfection reagent. Neither the scrambled control siRNA nor the negative control miRNA matched any human or mouse mRNA. For the transfection of all of the RNAi molecules purchased from Sigma-Aldrich into human fibroblasts, we used jetPRIME (Polyplus-transfection SA) as a transfection reagent with a high amount of RNAi molecules because the human fibroblasts exhibited a lower transduction efficiency of RNAi molecules compared with those of the HEK293T cells and Neuro2a cells, for which we used Lipofectamine 2000 (Life Technologies) as a transfection reagent. The transfected cells were cultured for 48 h before being processed for western blotting and RNA analysis.

Protein expression analysis. We did western blotting and densitometric analyses as previously described[12,14]. We used the following primary antibodies: AR-specific antibody (1:5,000, N20 or 1:5,000, H280; Santa Cruz), CELF2-specific antibody (1:5,000, ab50734; Abcam), α-tubulin–specific antibody (1:5,000, T9026; Sigma-Aldrich), GFP-specific antibody (1:5,000, M048-3; MBL), GFAP-specific antibody (1:2,000, 814369; Boehringer Manheim Biochemica), IGF-1–specific antibody (1:1,000, ab9572; Abcam) and cleaved caspase-3–specific antibody (1:2,000, 9661s; Cell Signaling Technology).

Quantitative real-time PCR. For cultured cells, the total RNA was extracted from HEK293T cells using the QIAzol Lysis Reagent (Qiagen) and reverse transcribed using Superscript VILO (Life Technologies). The complementary DNAs were then used for real time PCR using the SsoFast EvaGreen Supermix (Bio-Rad Laboratories). For mouse tissue analysis, the total RNA was isolated from the thoracic spinal cord and skeletal muscles of mice using the QIAzol Lysis Reagent (Qiagen) and reverse transcribed with the miScript Reverse-Transcription Kit (Qiagen). The complementary DNAs were then used for real time PCR using the SYBR Green Supermix (Qiagen). We did the amplification, detection and data analysis using a Bio-Rad iCycler system (Bio-Rad Laboratories). The crossing threshold values for the mRNAs of the individual genes were normalized to β-2-microglobulin (B2MG). The crossing threshold values for the miRNA of the individual genes were normalized to the U6 small nuclear RNA 2. Changes in the expression of mRNA and miRNA were expressed as a fold change relative to the control.

We used the following primers in this study. The sequences of the hsa-AR primers were: forward, 5′-GGCTATGAATGTCAGCCCAT-3′; reverse, 5′-TTGAGG CTAGAGAGCAAGGC-3′. These hsa-AR primers discriminated between the human AR mRNA and the mouse AR mRNA. The sequences of the mmu-AR primers were: forward, 5′-TGGGACCTTGGATGGAGAACTA-3′; reverse, 5′-ACAGATCAGGCAGGTCTTCTGG-3′. These mmu-AR primers discriminated between the mouse AR mRNA and the human AR mRNA. The sequences of the hsa-CELF2 primers were: forward, 5′-CTGGCGGGAAACAAACTCTG-3′; reverse, 5′-TCTAAGGCCTTGGCCTCCTC-3′. The sequences of the mmu-CELF2 primers were: forward, 5′-GCTGTGCGTTTGTCACATTTTC-3′; reverse, 5′-TGTCAGC AAACTTCACCACGAT-3′. The sequences of the hsa-B2MG primers were: forward, 5′-CTGAAGCTGACAGCATTCGG-3′; reverse, 5′-GTCAACTTCAATGT CGGATGGATG-3′. The sequences of the mmu-B2MG primers were: forward, 5′-AAGCCGAACATACTGAACTGC-3′; reverse, 5′-GTGTGAGCCAGGATATA GAAAGAC-3′. The sequences of the hsa-IGF-1 primers were: forward, 5′-GCTGT GATCTAAGGAGGCTGGA-3′; reverse, 5′- TTCCTGCACTCCCTCTACTTGCA TGGATG-3′. The primers used for the detection of miR-196a, miR -196b and U6 small nuclear RNA 2 were the Hs_miR-196a_1 miScript Primer Assay (Qiagen), the Hs_miR-196b_2 miScript Primer Assay (Qiagen) and the Hs_RNU6-2_1 miScript Primer Assay (Qiagen), respectively.

Immunoprecipitation-coupled qRT-PCR. We did coimmunoprecipitation using an affinity-purified CELF2 antibody (15 μg per sample, ab50734; Abcam) followed by RNA isolation using the RiboCluster Profiler RIP-Assay kit (MBL International Corporation) according to the manufacturer's suggested protocols. Rabbit immunoglobulin G, supplied by the manufacturer, was used as a control, and the immunoprecipitated RNA was converted to cDNA using Superscript VILO (Life Technologies) and analyzed by qRT-PCR for the differential expression of AR mRNA using the following primers: forward, 5′-GGCTATGAATGTCAGCCCAT-3′; reverse, 5′-TTGAGGCT AGAGAGCAAGGC-3′.

RNA stability assay. We added actinomycin D (10 mg ml^{-1} final concentration), a potent inhibitor of mRNA synthesis, to the HEK293T cells at 24 h after co-transfection of DNA plasmid and RNAi molecules. The total RNA was extracted from the cells at 0–4 h after treatment, and the RNA was then subjected to qRT-PCR as described above. The data are presented as values relative to the levels of expression detected in the transfected cells harvested at the time of actinomycin D treatment.

miRNA microarray analysis. The total RNA was extracted from the thoracic spinal cord of transgenic SBMA mice (AR-97Q) and wild-type mice (AR-24Q)

at 15 weeks of age and used for the miRNA microarray analysis conducted by TaKaRa Bio. Each group consisted of two mice.

miRNA *in situ* hybridization. To investigate the cell-specific distribution of miRNA in mouse spinal tissues, we did *in situ* hybridization using 5′- and 3′-end digoxigenin (DIG)-labeled locked nucleic acid (LNA)-modified DNA oligonucleotides complementary to the mature miRNA (Exiqon). In this study, we examined the global expression of miR-196a in mouse tissue sections that had been prepared as previously described[13–15,33]. The LNA-miR-196a and LNA-scrambled oligonucleotides (negative control) were used in this analysis.

We did the *in situ* hybridization of mouse tissue sections using a Ventana Discovery system (Ventana Medical Systems). Briefly, 5′- and 3′-end DIG-labeled LNA probes were stained with digoxigenin-AP–specific Fab fragments (1:800, 1093274; Roche). The sections were then counterstained using Red Counterstain II (780-2218; Ventana), and the signals were visualized under a standard light microscope.

Development of the AAV vector with simultaneous expression of miRNA and EGFP. The AAV vector plasmids contained an expression cassette consisting of a human cytomegalovirus immediate-early promoter, followed by cDNA encoding EGFP, miR-196a or the miR-mock sequence, and a woodchuck hepatitis virus post-transcriptional regulatory element between the inverted terminal repeats of the AAV3 genome. We synthesized the AAV9 *vp* cDNA, and this sequence was identical to that previously described[34] except for the substitution of adenine with thymidine at position 1337, which introduced an amino acid change from tyrosine to phenylalanine at position 446 (ref. 23). The recombinant AAV vectors were produced by transient transfection of HEK293 cells using the vector plasmid, an AAV3 *rep* and AAV9 *vp* expression plasmid and an adenoviral helper plasmid, pHelper (Stratagene), as previously described[35]. We purified the recombinant viruses by isolation from two sequential continuous CsCl gradients, and then the viral titers were determined by qRT-PCR. The cDNA sequences of miR-196a and miR-mock are as follows. miR-196a: 5′-TGAGCCGGGACTGTTGAGTGAAGTAGGT AGTTTCATGTTGTTGGGCCTGGCTTTCTGAACACAACGACATCAAA CCACCTGATTCATGGCAGTTACTGCTTC-3′. miR-mock: 5′-GTATTGC GTCTGTACACTCACCGTTTTGGCCACTGACTGACGGTGAGTGCAG ACGCAATA-3′.

The neurological and behavioral assessment of the SBMA model mice. We generated and maintained the AR-24Q and AR-97Q mice as previously described[12]. All of the animal experiments were carried out in accordance with the National Institutes of Health Guide for the Care and Use of Laboratory Animals and were approved by the Nagoya University Animal Experiment Committee. We did the mouse rotarod task and cage activity assessment as described previously[12,14]. The investigators who carried out the behavioral assessments were blinded to the treatment conditions.

Immunohistochemistry, immunofluorescence, histochemistry and histopathology. The preparation of the tissue sections, immunohistochemistry, immunofluorescence and histopathology were done as previously described[11–15, 33].

To quantify the 1C2-positive cells, we counted the 1C2-positive cells within the thoracic spinal cord and quadriceps femoris muscle for each individual mouse as previously described[12,14]. For choline acetyltransferase immunolabeling, the sections were first microwaved for 20 min in 50 mM citrate buffer, pH 6.0. For polyglutamine (1C2 antibody) immunolabeling, the sections were treated with formic acid for 5 min at room temperature. We treated all of the specimens with TNB blocking buffer (PerkinElmer) before incubation with primary antibodies. The immunohistochemical sections were then imaged using an optical microscope (BX51, Olympus), and the immunofluorescent specimens were photographed using an upright microscope (LSM710, Zeiss). We used the following primary antibodies: choline acetyltransferase–specific antibody (1:100, AB144; Millipore), mouse GFP-specific antibody (1:200, M048-3; MBL), mouse expanded polyQ antibody (1:10,000, 1C2; Millipore) and mouse GFAP-specific antibody (1:1,000, 814369; Boehringer Manheim Biochemica). The primary antibodies were probed with biotinylated anti–species-specific IgG secondary antibodies (Vector Laboratories), and the immune complexes were visualized using streptavidin–horseradish peroxidase (Dako) and 3,3′-diaminobenzidine as a substrate. We used Alexa-conjugated secondary antibodies (Life Technologies) for immunofluorescence. We assessed the size of the motor neuron in the thoracic spinal cord of the SBMA mice treated with AAV-miR-196a or AAV-miR-mock as previously described[33]. The stained sections were then examined and imaged using a BIOREVO BZ-9000 system (Keyence). To assess the GFAP expression levels in the thoracic spinal anterior horn cells, we quantified the immunohistochemistry signal intensities in at least ten transverse sections obtained from each mouse. The images of individual anterior horn on transverse sections of thoracic spinal cord with signals for GFAP were captured at the desired magnification and stored using image software (Keyence). The levels of GFAP staining in the images were quantitatively analyzed using image analysis software (Dynamic cell count BZ-HIC software, Keyence). The signal intensities were expressed as individual intracellular areas of GFAP staining (μm^2) in the unilateral thoracic spinal anterior horn.

Assay of serum testosterone levels in SBMA mice. We sacrificed SBMA mice treated with AAV-miR-196a or AAV-miR-mock at 12 weeks of age, collected 1 ml of blood by cardiocentesis and conducted an assay for serum testosterone levels using a radioimmunoassay (Mitsubishi Kagaku Bio-Clinical Laboratories).

The fibroblasts and thoracic spinal cords of patients. We obtained biopsy specimens of fibroblasts of scrotal skin from three patients genetically diagnosed with SBMA and three disease control subjects. The CAG repeat lengths of the patients with SBMA were 48, 50 and 52. The disease control subjects included three male individuals who were diagnosed with a cerebrovascular disease.

We obtained autopsy specimens of the thoracic spinal cord from three patients genetically diagnosed with SBMA (52-, 66- and 78-year-old males) and from disease control subjects (58-, 61- and 75-year-old males). The CAG repeat lengths of three patients with SBMA were 48, 49 and 50, respectively. The disease control subjects included individuals diagnosed with Parkinson's disease ($n = 2$) and dementia with Lewy body disease ($n = 1$). The collection of human tissues and their use for this study were approved by the Ethics Committee of Nagoya University Graduate School of Medicine. We obtained informed consent from the patients.

The pulse-chase labeling assay. HEK293T cells were transfected as previously described, starved for 1 h and then labeled for an additional 1 h with 150 mCi ml^{-1} of EXPRE^{35}S^{35}S Protein Labeling Mix [^{35}S] (PerkinElmer Life & Analytical Sciences). We chased the HEK293T cells for the indicated time intervals. We then did immunoprecipitation using equivalent amounts of protein lysates as previously described[14] and analyzed the expression levels using phosphorimaging (Typhoon 8600 phosphorimager; Amersham) and Image Gauge software, version 4.22 (Fujifilm).

The apoptosis assay. We plated Neuro2a neuronal lineage cells onto six-well dishes and co-transfected each dish with 25 nM synthetic miR-196a using Lipofectamine 2000 (Life Technologies) according to the manufacturer's instructions. After 24 h, we treated the Neuro2a cells with 1 μM staurosporine, a major inducer of apoptosis, for 6 h. Next, we processed and probed the western blots with a cleaved caspase-3 antibody. The effect of miR-196a on apoptosis in the Neuro2a cells was then assessed by the change in the relative expression levels of cleaved caspase-3 protein.

Statistical analyses. We analyzed the results by unpaired *t* tests, Dunnett tests and two-way ANOVA followed by Bonferroni tests for individual paired comparison using IBM SPSS statistics version 19 for Windows (IBM). We used log-rank tests for the assessment of the survival rate in **Fig. 3d** using IBM

SPSS statistics version 19 for Windows (IBM). *P* values of less than 0.05 were considered statistically significant.

32. Kobayashi, Y. *et al.* Chaperones Hsp70 and Hsp40 suppress aggregate formation and apoptosis in cultured neuronal cells expressing truncated androgen receptor protein with expanded polyglutamine tract. *J. Biol. Chem.* **275**, 8772–8778 (2000).
33. Katsuno, M. *et al.* Disrupted transforming growth factor-β signaling in spinal and bulbar muscular atrophy. *J. Neurosci.* **30**, 5702–5712 (2010).
34. Gao, G. *et al.* Clades of adeno-associated viruses are widely disseminated in human tissues. *J. Virol.* **78**, 6381–6388 (2004).
35. Li, X.G. *et al.* Viral-mediated temporally controlled dopamine production in a rat model of Parkinson disease. *Mol. Ther.* **13**, 160–166 (2006).

doi:10.1038/nm.2791

OPEN ACCESS Freely available online

PLOS ONE

c-Abl Inhibition Delays Motor Neuron Degeneration in the G93A Mouse, an Animal Model of Amyotrophic Lateral Sclerosis

Ryu Katsumata[1], Shinsuke Ishigaki[1,2,3], Masahisa Katsuno[1], Kaori Kawai[1], Jun Sone[1], Zhe Huang[1], Hiroaki Adachi[1], Fumiaki Tanaka[1], Fumihiko Urano[2,4], Gen Sobue[1,3]*

1 Department of Neurology, Nagoya University Graduate School of Medicine, Tsurumai-cho, Showa-ku, Nagoya, Japan, **2** Program in Gene Function and Expression, University of Massachusetts Medical School, Worcester, Massachusetts, United States of America, **3** Core Research for Evolutional Science and Technology, Japan Science and Technology Agency, Saitama, Japan, **4** Program in Molecular Medicine, University of Massachusetts Medical School, Worcester, Massachusetts, United States of America

Abstract

Background: Amyotrophic lateral sclerosis (ALS) is a fatal neurodegenerative disease characterized by progressive death of motor neurons. Although the pathogenesis of ALS remains unclear, several cellular processes are known to be involved, including apoptosis. A previous study revealed the apoptosis-related gene c-Abl to be upregulated in sporadic ALS motor neurons.

Methodology/Findings: We investigated the possibility that c-Abl activation is involved in the progression of ALS and that c-Abl inhibition is potentially a therapeutic strategy for ALS. Using a mouse motor neuron cell line, we found that mutation of Cu/Zn-superoxide dismutase-1 (SOD1), which is one of the causative genes of familial ALS, induced the upregulation of c-Abl and decreased cell viability, and that the c-Abl inhibitor dasatinib inhibited cytotoxicity. Activation of c-Abl with a concomitant increase in activated caspase-3 was observed in the lumbar spine of G93A-SOD1 transgenic mice (G93A mice), a widely used model of ALS. The survival of G93A mice was improved by oral administration of dasatinib, which also decreased c-Abl phosphorylation, inactivated caspase-3, and improved the innervation status of neuromuscular junctions. In addition, c-Abl expression in postmortem spinal cord tissues from sporadic ALS patients was increased by 3-fold compared with non-ALS patients.

Conclusions/Significance: The present results suggest that c-Abl is a potential therapeutic target for ALS and that the c-Abl inhibitor dasatinib has neuroprotective properties *in vitro* and *in vivo*.

Citation: Katsumata R, Ishigaki S, Katsuno M, Kawai K, Sone J, et al. (2012) c-Abl Inhibition Delays Motor Neuron Degeneration in the G93A Mouse, an Animal Model of Amyotrophic Lateral Sclerosis. PLoS ONE 7(9): e46185. doi:10.1371/journal.pone.0046185

Editor: Thomas H. Gillingwater, University of Edinburgh, United Kingdom

Received March 21, 2012; **Accepted** August 28, 2012; **Published** September 25, 2012

Funding: This work was supported by a Center-of-Excellence (COE) grant from the Ministry of Education, Culture, Sports, Science and Technology of Japan [http://w3serv.nagoya-u.ac.jp/coemed/en/index.html]; a Grant-in-Aid for Scientific Research on Innovated Areas "Foundation of Synapse and Neurocircuit Pathology" [http://www.tmd.ac.jp/mri/shingakujutu/index-e.html], and Grant-in-Aids from Ministry of Education, Culture, Sports, Science, and Technology of Japan [http://www.jsps.go.jp/english/e-grants/index.html]; grants from the Ministry of Health, Labor and Welfare of Japan [http://www.mhlw.go.jp/english/policy/other/research-projects/index.html]; and Core Research for Evolutional Science and Technology (CREST) from the Japan Science and Technology Agency (JST) [http://www.sss.jst.go.jp/english/index.html]. The funders had no role in study design, data collection and analysis, decision to publish, or preparation of the manuscript.

Competing Interests: The authors have declared that no competing interests exist.

* E-mail: sobueg@med.nagoya-u.ac.jp

Introduction

Amyotrophic lateral sclerosis (ALS) is a neurodegenerative disease characterized by selective loss of upper and lower motor neurons in the cerebral cortex, brain stem, and spinal cord [1,2]. Many genes have been identified as involved in familial ALS cases, including Cu/Zn-superoxide dismutase-1 (SOD1) [3,4,5]. Approximately 5–10% of ALS cases are familial, and 20% of familial ALS cases are associated with mutations in the SOD1 gene [3]. Several hypotheses for the pathogenesis of ALS have been proposed, including oxidative stress, glutamate excitotoxicity, mitochondrial dysfunction, and neuroinflammation, all of which eventually lead to the death of motor neurons [6,7,8,9]. Many studies using mutant SOD1 transgenic animals have explored the precise cellular mechanisms of motor neuron death; however, no therapeutic drugs have been developed to date except for riluzole, which has only limited effects. Since most cases of ALS are sporadic, the development of ALS drug therapies based on the pathology of sporadic ALS (sALS) is feasible.

Previously, we performed microarray analyses combined with laser-capture microdissection to investigate the gene expression profiles of spinal motor neurons isolated from autopsied patients with sALS [10]. We found altered expression of many genes, including dynactin 1, early growth response-3, acetyl-CoA transporter, death receptor 5, and cyclin C [10,11]. In that study, a 4.41-fold increase in the amount of c-Abl mRNA was detected in the motor neurons of sALS patients [10]. These findings raised the

possibility that upregulation of c-Abl in motor neurons contributes to motor neuron degeneration and that activation of this pathway may be one of the pathologic features of ALS.

c-Abl is a ubiquitous non-receptor tyrosine kinase that was originally identified as the cellular homolog of the v-abl gene, an oncogene carried by the Abelson murine leukemia virus [12]. Bcr-Abl hybrid protein, which is one of the oncogenic forms of c-Abl fusion kinase, causes chronic myelogenous leukemia (CML) and Philadelphia chromosome-positive adult acute lymphoblastic leukemia (Ph+ALL) [13,14]. The kinase activity of c-Abl is regulated by phosphorylation. Tyrosine 245 (Tyr245) and tyrosine 412 (Tyr412) are well-established regulatory phospho-tyrosine residues that are required for c-Abl activation [15]. In response to various stimuli, c-Abl regulates cytoskeletal rearrangement, cell migration, cell-cell adhesion, cell proliferation, and apoptosis [16,17,18,19,20]. On exposure to stressors, such as DNA damage or oxidative stress, c-Abl has been implicated in cell growth arrest and caused apoptotic cell death in association with p73 [21,22], PKC delta [23], and CDK5 [24,25]. Recently, neural functions of c-Abl have also been described: c-Abl participates in neuronal development and neurite outgrowth [26,27], and has also been implicated in the pathogenesis of Alzheimer's disease [28,29].

In the present study, we investigated c-Abl activation in a mutant SOD1 transgenic ALS mouse model and in sALS patients, and we demonstrated that the c-Abl inhibitor dasatinib has a protective effect on motor neuron degeneration in G93A-SOD1 transgenic ALS mice (G93A mice).

Results

Inducible expression of wild-type and mutant SOD1 in NSC-34 cells

To investigate the expression and activity levels of c-Abl in human mutant SOD1-expressing motor neurons, we established an inducible system of NSC-34 cells able to express either human wild-type or mutant (G93A, G85R) SOD1 protein. Western blot analysis confirmed that myc-tagged human SOD1 proteins were induced by doxycycline in these cell lines (Fig. 1A). Myc-tagged human SOD1 demonstrated lower mobility than mouse endogenous SOD1. NSC-34 cells were well differentiated in low-serum medium with extended neuritic processes, a morphological marker of neuronal cell maturation and differentiation [30]. As a motor neuron-mimicking model, we used NSC-34 cells with serum-free medium to measure cytotoxicity. Cell viability was examined using the MTS-based cell proliferation assay at 48 h after the induction of SOD1 proteins, and we found that both G93A and G85R mutant SOD1s significantly decreased cell viability in comparison with wild-type SOD1 ($P<0.05$ for G93A, $P<0.01$ for G85R) (Fig. 1B). The cytotoxicity of mutant SOD1s was also measured by lactate dehydrogenase (LDH) release assay at 48 h after the induction of SOD1 proteins. The results demonstrated that both G93A and G85R mutant SOD1s significantly increased cytotoxicity in comparison with wild-type SOD1 ($P<0.05$ for G93A, $P<0.01$ for G85R) (Fig. 1C).

c-Abl activation caused by mutant SOD1 in NSC-34 cells

We then investigated whether overexpression of mutant SOD1s influenced the expression of c-Abl. Western blot analysis revealed that the expression of c-Abl was greater in cells expressing mutant SOD1s (G93A and G85R) than cells expressing wild-type SOD1 (Fig. 2A). These differences were much more prominent when phospho-specific antibodies for each of 2 distinct tyrosine residues (Tyr245 and Tyr412) were used for the western blot analysis. Densitometric analysis confirmed that mutant SOD1 significantly increased the expression and phosphorylation of c-Abl ($P<0.05$) (Fig. 2B). Increased c-Abl mRNA expression in cells overexpressing mutant SOD1s was also confirmed by quantitative RT-PCR (Fig. 2C).

Dasatinib attenuates the cytotoxicity of mutant SOD1s in NSC-34 cells

To examine whether the inhibition of c-Abl kinase influenced the cytotoxicity of mutant SOD1s, we evaluated the effect of dasatinib, a blood-brain barrier (BBB)-permeable c-Abl inhibitor, on c-Abl activity in NSC-34 cells expressing different forms of SOD1. Cells overexpressing SOD1 were treated with increasing concentrations of dasatinib for 24 h and analyzed by western blotting. Dasatinib effectively suppressed the phosphorylation of c-Abl in all cell lines (Fig. 3A). Since dasatinib is a dual c-Abl/c-Src kinase inhibitor [31], in order to clarify the specificity of c-Abl for motor neuronal cytotoxicity, we also performed cell proliferation and cell death assays with SU6656, which preferentially inhibits c-Src compared to c-Abl. SU5666 effectively suppressed the phosphorylation of c-Src in all cell lines (Fig. 3A). Cell viability and cell death assays confirmed that dasatinib significantly reduced the cytotoxicity of mutant SOD1s ($P<0.05$), whereas SU6656 did not (Fig. 3B, C).

Upregulation and activation of c-Abl in G93A mice

To determine whether c-Abl upregulation also occurs in G93A mice, we measured mRNA and protein levels of c-Abl in the lumbar spinal cords of G93A and control mice at age 10 weeks (pre-symptomatic stage), 14 weeks (symptomatic stage), and 18 weeks (terminal stage) by quantitative RT-PCR and western blot analyses. The protein expression of c-Abl in the lumbar spinal cords of G93A mice was increased as early as 10 weeks compared with control littermates (Fig. 4A). A remarkable increase in the phosphorylation of c-Abl was also evident even at the pre-clinical stage of 10 weeks. The increase in c-Abl protein was paralleled by an induction of c-Abl mRNA in the spinal cords of G93A mice (Fig. 4B). Consistent with the western blot analyses and quantitative RT-PCR, immunoreactivity for c-Abl and phosphorylated c-Abl (Tyr245 and Tyr412) was increased in the lumbar spinal neurons of G93A mice compared with those of control littermates (Fig. 4C). We quantified the signal intensity of phosphorylated c-Abl immunofluorescence in motor neurons (Tyr412 and Tyr245) using Image J software. Phosphorylated c-Abl immunoreactivity in G93A mice was significantly increased compared to control mice with both antibodies ($P<0.01$), which indicated that c-Abl was activated at an early stage of disease in this mouse model of ALS (Fig. S1).

The effect of dasatinib on survival and disease progression in G93A mice

Survival of G93A mice was improved by dasatinib at a dose of 25 mg/(kg·day) compared with vehicle treatment ($P<0.01$, 25 mg/(kg·day) vs. vehicle), whereas a lower dose of dasatinib (5 mg/(kg·day)) had no significant effect on life span (Fig. 5). Weight loss was also ameliorated by dasatinib at a dose of 25 mg/(kg·day) compared with vehicle treatment (Fig. 5, 2-way ANOVA, $P<0.01$, 25 mg/(kg·day) vs. vehicle). The administration of dasatinib at 25 mg/(kg·day) similarly alleviated motor dysfunction measured by grip strength (2-way ANOVA, $P<0.01$, 25 mg/(kg·day) vs. vehicle). Dasatinib did not significantly ameliorate the physical function assessed by rotarod, although a beneficial tendency was observed. Dasatinib did not alter the neuromuscular

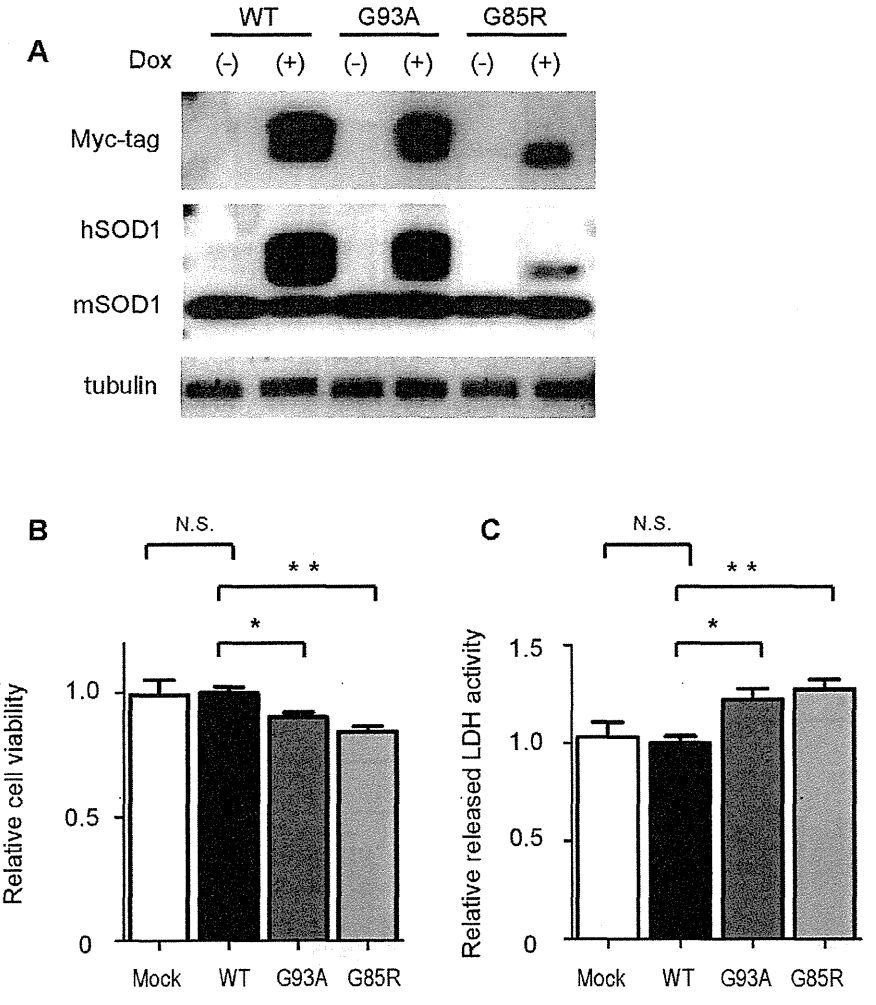

Figure 1. Inducible expression system of wild-type and mutant SOD1s in NSC-34 cells. A: NSC-34 cells were stably transduced with an inducible lentivirus expressing human Myc-tagged wild-type or mutant SOD1 protein. Cells were cultured with or without doxycycline (Dox, 2 μg/ml) for 48 h to induce SOD1 protein. Tubulin is shown as a loading control. hSOD1 and mSOD1 indicate human SOD1 and mouse endogenous SOD1, respectively. B: Cell viability assay based on the MTS method showed that overexpression of both types of mutant SOD1, G93A and G85R, caused cytotoxicity in serum-free culture medium. Mock indicates mock-transfected NSC-34 cells. Data are presented as mean ± SEM. Statistics were evaluated using 1-way ANOVA with Dunnett's post-hoc test. *$P<0.05$, **$P<0.01$ C: Cytotoxicity detection assay using the LDH release method revealed that overexpression of both types of mutant SOD1, G93A and G85R, caused cytotoxicity in serum-free culture medium. Data are presented as mean ± SEM. Statistics were evaluated using 1-way ANOVA with Dunnett's post-hoc test. *$P<0.05$, **$P<0.01$.
doi:10.1371/journal.pone.0046185.g001

function or body weight of non-transgenic littermates at any of the doses tested (data not shown).

The effect of dasatinib on motor neuron survival and innervation status of neuromuscular junctions (NMJs) in G93A mice

Paraffin-embedded sections of the lumbar spinal cord (L1-3) from 120-day-old mice were analyzed immunohistochemically using anti-choline acetyltransferase (ChAT) antibody (Fig. 6A). The number of ChAT-positive motor neurons in the lumbar spinal cord was significantly preserved in mice treated with dasatinib at doses of 15 mg/(kg·day) or higher compared with vehicle-treated control mice ($P<0.05$) (Fig. 6B). To evaluate changes in the size of ChAT-positive motor neurons, we quantified the cell body areas of ChAT-positive motor neurons using Image J software. The size of motor neurons in dasatinib-treated mice was significantly preserved compared to vehicle-treated controls ($P<0.05$) (Fig. 6C). To investigate the innervation status of neuromuscular junctions (NMJs), frozen quadriceps femoris specimens were collected from 120-day-old mice and stained with alpha-bungarotoxin (BuTX) (red) and anti-synaptophysin (green) or anti-SMI31 (green) antibodies (Fig. 6D). We observed BuTX-positive NMJs (treated and control groups; n = 3 mice per group, 100 NMJs per mouse) using confocal laser scanning microscopy and counted double- (red and green) or single (red)-immunostained NMJs. Figure 6E summarizes the ratio of double-immunostained (innervated) NMJs to total NMJs. Dasatinib significantly ameliorated the destruction of NMJ innervation in G93A mice at doses of 5, 15, and 25 mg/(kg·day) compared to vehicle treatment ($P<0.05$) (Fig. 6E).

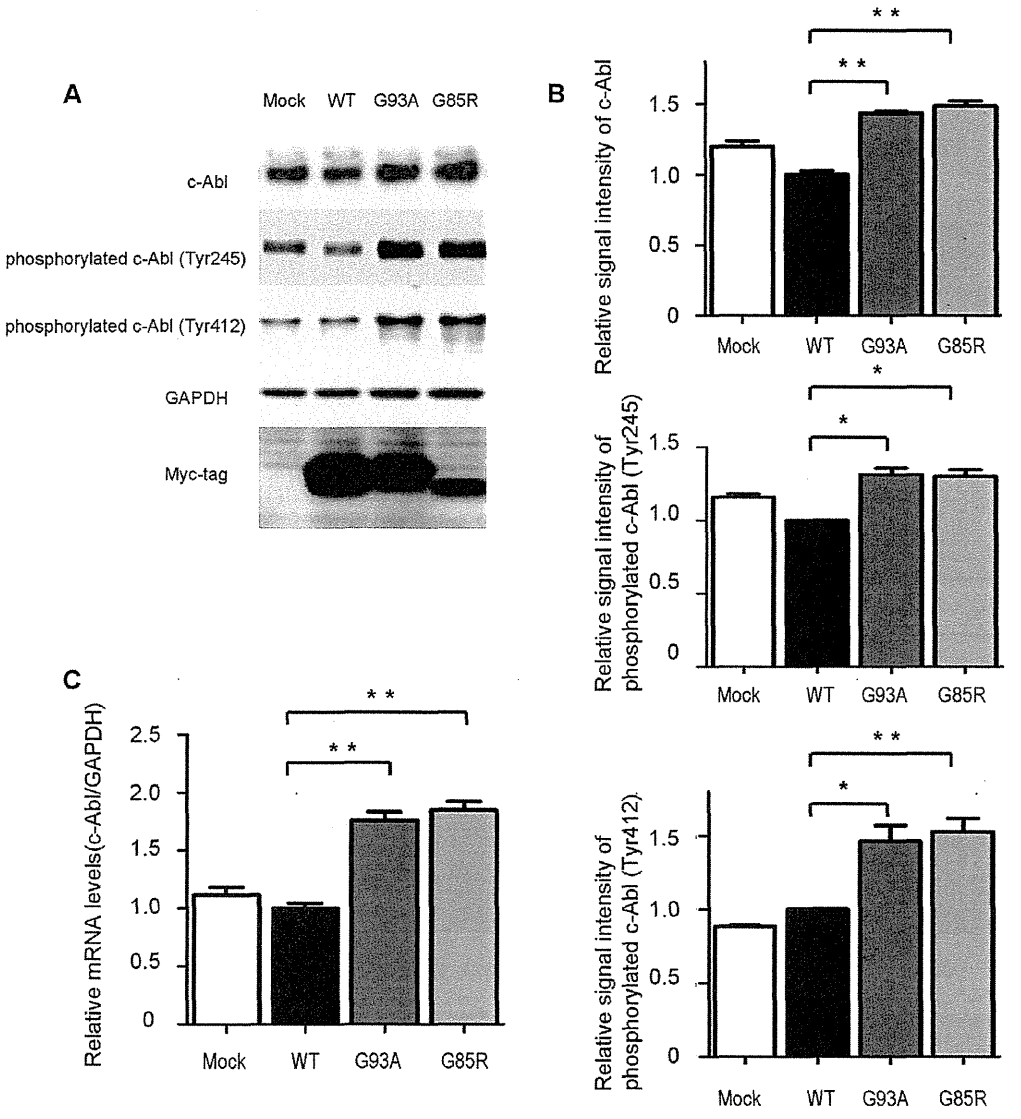

Figure 2. Activation of c-Abl caused by mutant SOD1 overexpression. A: Total c-Abl and phospho-c-Abl (Tyr245 and Tyr412) protein levels in NSC-34 cells overexpressing human wild-type and mutant SOD1 protein were measured by western blotting. GAPDH is shown as a loading control. Cells were cultured with doxycycline (Dox, 2 μg/ml) in serum-free culture medium for 48 h. B: Densitometric analysis (n = 3 per group) of the results shown in Fig. 2A demonstrated that both types of mutant SOD1, G93A and G85R, significantly increased the amount of total c-Abl protein and facilitated phosphorylation at both c-Abl sites, Tyr245 and Tyr412. Data are presented as mean ± SEM. Statistical analysis was performed using 1-way ANOVA with Dunnett's post-hoc test. *$P<0.05$, **$P<0.01$. C: Expression levels of c-Abl mRNA were measured by quantitative RT-PCR in NSC-34 cells overexpressing wild-type or mutant human SOD1 (n = 4 per group). Cells were cultured with doxycycline (Dox, 2 μg/ml) in serum-free culture medium for 48 h. Overexpression of both types of mutant SOD1 significantly increased the c-Abl mRNA level compared with overexpression of wild-type SOD1 ($P<0.01$). Data shown are ratios (mean ± SEM) of the c-Abl mRNA levels in NSC-34 cells overexpressing wild type SOD1 (n = 6). Statistics were evaluated using 1-way ANOVA with Dunnett's post-hoc test. **$P<0.01$.
doi:10.1371/journal.pone.0046185.g002

Dasatinib reduces phosphorylation of c-Abl and the activated form of caspase-3 in G93A mice

To assess the effect of dasatinib on the central nervous system (CNS), we performed western blot analyses using the spinal cords of G93A mice and control littermates treated with dasatinib or vehicle (Fig. 7). The levels of phosphorylated c-Abl (Tyr245) were decreased in a dose-dependent manner in G93A mice treated with dasatinib. In addition, activated caspase-3 was decreased in mice treated with high-dose dasatinib (Fig. 7). Quantification of immunofluorescence revealed that phosphorylated c-Abl (Tyr412) levels were significantly decreased in dasatinib-treated G93A mice at doses of 15 mg/(kg·day) or higher compared with vehicle-treated control mice ($P<0.01$) (Fig. S2). These results suggest that dasatinib protects motor neurons from mutant SOD1-induced neuronal cell death by inhibiting apoptosis.

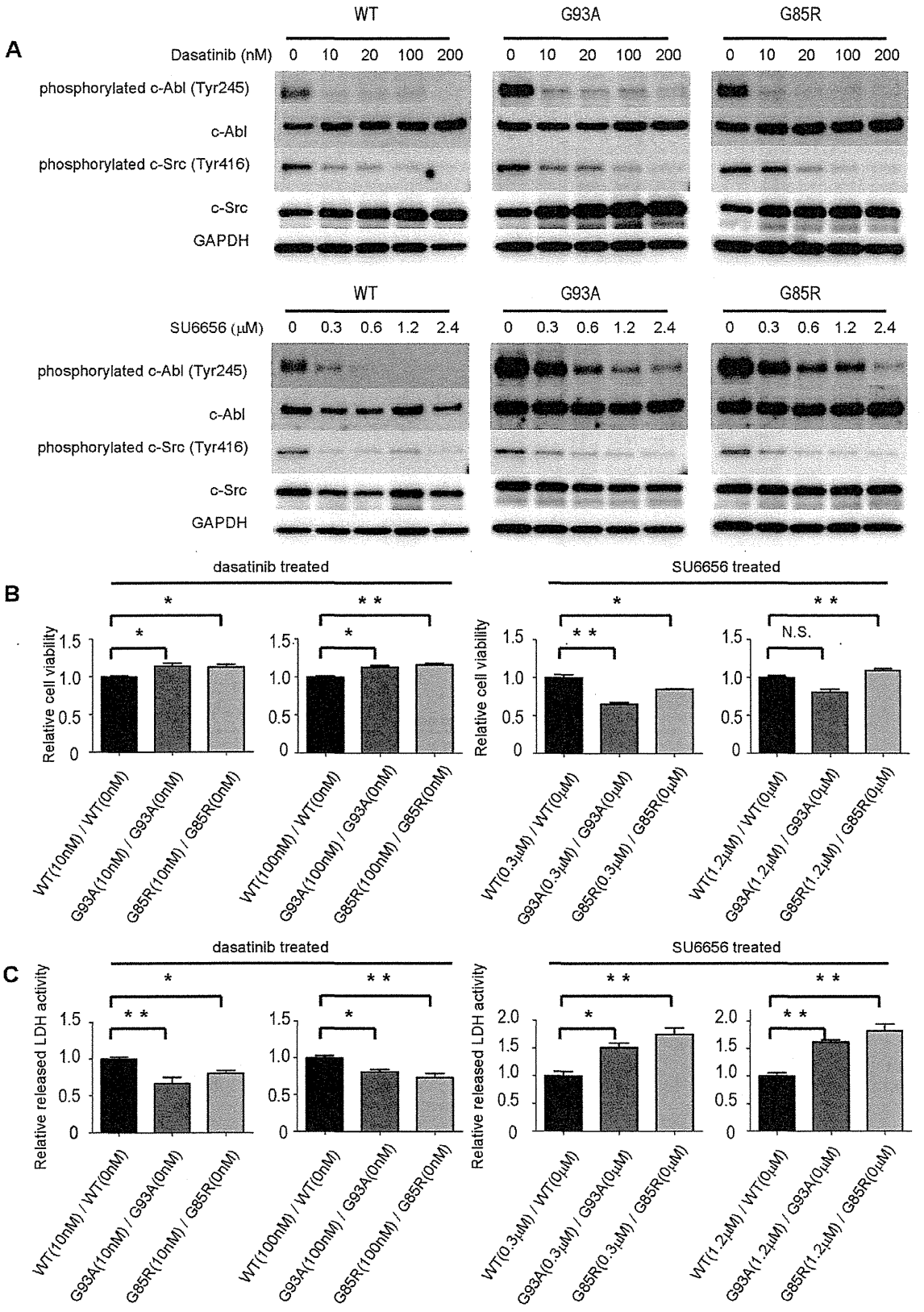
A
WT
G93A
G85R
Dasatinib (nM) 0 10 20 100 200
phosphorylated c-Abl (Tyr245)
c-Abl
phosphorylated c-Src (Tyr416)
c-Src
GAPDH
SU6656 (μM) 0 0.3 0.6 1.2 2.4
B
dasatinib treated
SU6656 treated
Relative cell viability
N.S.
WT(10nM) / WT(0nM)
G93A(10nM) / G93A(0nM)
G85R(10nM) / G85R(0nM)
WT(100nM) / WT(0nM)
G93A(100nM) / G93A(0nM)
G85R(100nM) / G85R(0nM)
WT(0.3μM) / WT(0μM)
G93A(0.3μM) / G93A(0μM)
G85R(0.3μM) / G85R(0μM)
WT(1.2μM) / WT(0μM)
G93A(1.2μM) / G93A(0μM)
G85R(1.2μM) / G85R(0μM)
C
Relative released LDH activity

Figure 3. Dasatinib reduces cytotoxicity of mutant SOD1s in NSC-34 cells. A: Protein levels of phosphorylated c-Abl (Tyr245), c-Abl, phosphorylated c-Src (Tyr416), c-Src, and GAPDH in NSC-34 cells overexpressing human wild-type or mutant SOD1s treated with various concentrations of dasatinib or SU6656 were measured by western blot. Cells were cultured in serum-free culture medium with doxycycline (Dox, 2 μg/ml), and western blot was performed at 24 h after dasatinib or SU6656 addition. B: Cells were grown in 96-well collagen-coated plates (3,500 cells per well) with doxycycline (Dox, 2 μg/ml) in culture medium containing 10% FBS for 16 h. Culture medium was then replaced with 1% FBS-containing medium including the indicated concentrations of dasatinib and 2 μg/ml doxycycline (Dox). MTS assays were performed at 24 h after addition of dasatinib or SU6656. Viability was measured as the level of absorbance at 490 nm. Absorbance at 490 nm was expressed as the mean ± SEM (n = 6). Ratios of relative cell viability based on the MTS assay were calculated to determine the beneficial effect of dasatinib in mutant cells overexpressing SOD1s. Absorbance at 490 nm was standardized relative to the absorbance at each corresponding time point for 0 nM dasatinib. Cell viability assay confirmed that dasatinib significantly reduced the cytotoxicity of mutant SOD1s, whereas SU6656 did not. Statistics were evaluated using 1-way ANOVA with Dunnett's post-hoc test. *$P<0.05$, **$P<0.01$. C: Cells were grown in 96-well collagen-coated plates (3,500 cells per well) with doxycycline (Dox, 2 μg/ml) in culture medium containing 10% FBS for 16 h. Culture medium was then replaced with 1% FBS-containing medium with the indicated concentrations of dasatinib and 2 μg/ml doxycycline (Dox). LDH assays were performed at 24 h after dasatinib or SU6656 addition. Cytotoxicity was measured as the level of absorbance at 490 nm. Ratios of relative LDH release were calculated to determine the beneficial effect of dasatinib in mutant cells overexpressing SOD1s. Absorbance at 490 nm was standardized relative to the absorbance at each corresponding time point for 0 nM dasatinib. LDH assay confirmed that dasatinib significantly reduced the cytotoxicity of mutant SOD1s, whereas SU6656 did not. Values represent the mean ± SEM of the ratio of LDH release (n = 4). Statistics were evaluated using 1-way ANOVA with Dunnett's post-hoc test. *$P<0.05$, **$P<0.01$.
doi:10.1371/journal.pone.0046185.g003

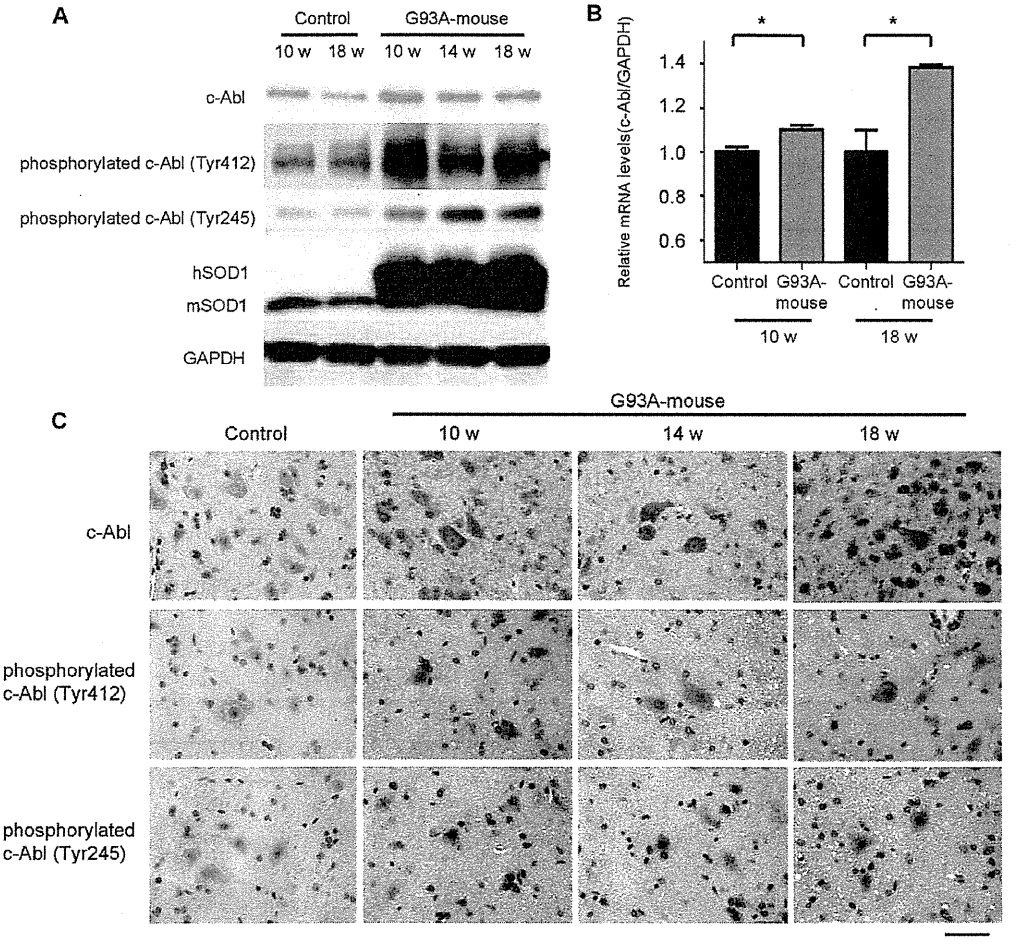

Figure 4. c-Abl upregulation and activation in G93A mice. A: Protein levels of phosphorylated c-Abl (Tyr245 and Tyr412) and c-Abl were analyzed by western blot using spinal cord protein extracts from control non-transgenic and G93A mice at the indicated ages. GAPDH is shown as a loading control. hSOD1 and mSOD1 indicate human SOD1 and mouse endogenous SOD1, respectively. B: c-Abl mRNA levels in the spinal cords of G93A mice and control littermates (age 10 and 18 weeks; n = 4 per group) were measured by quantitative RT-PCR. Data shown are the ratios of the c-Abl mRNA level in each group relative to that in control littermates. c-Abl mRNA was significantly increased in the spinal cords of G93A mice in both age groups compared with control littermates ($P<0.05$). Data are presented as mean ± SEM. Statistics were evaluated using Student's *t* test. *$P<0.05$. C: Distribution of total and phosphorylated c-Abl proteins was analyzed by immunohistochemical staining of paraffin-embedded spinal cord sections from G93A mice (10, 14, and 18 weeks old) and control littermates (20 weeks old) using antibodies directed against c-Abl, phosphorylated c-Abl (Tyr245), and phosphorylated c-Abl (Tyr412). Scale bar: 50 μm.
doi:10.1371/journal.pone.0046185.g004

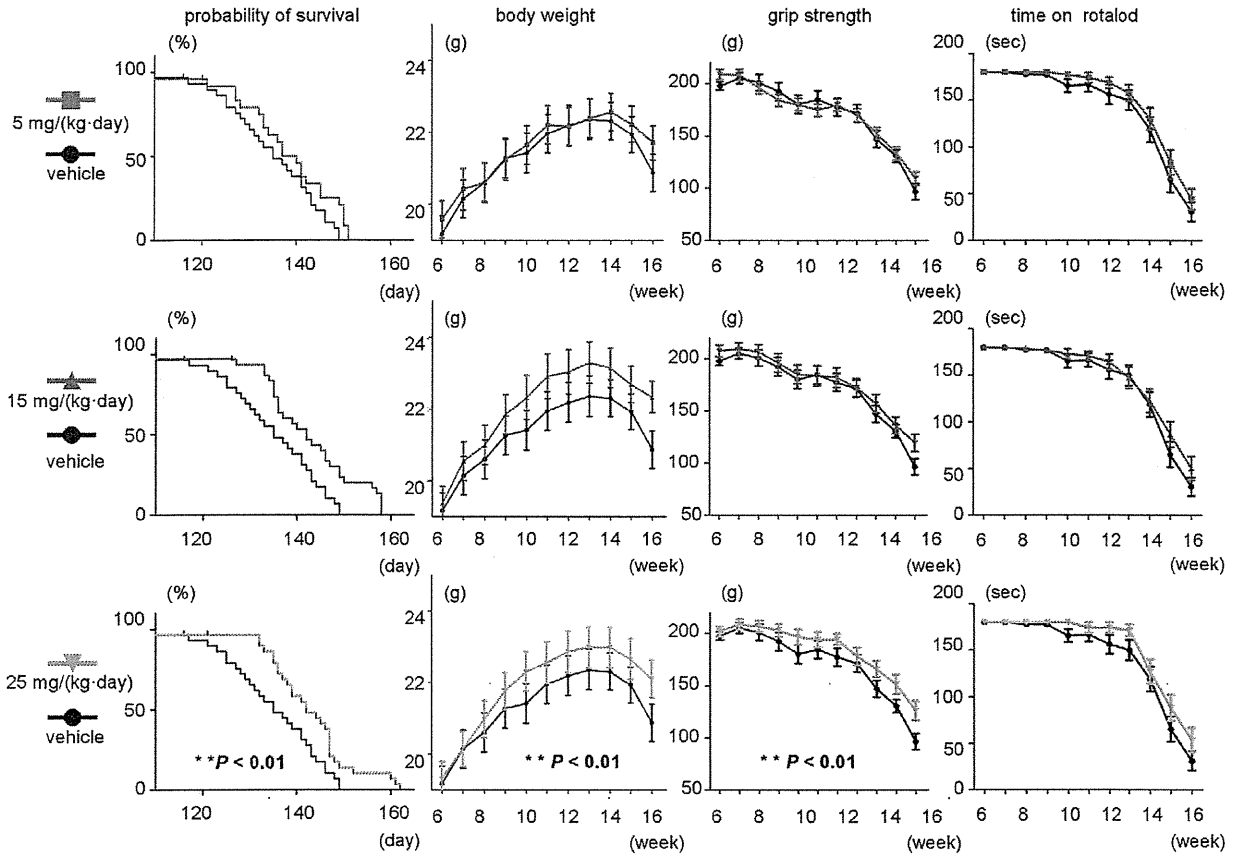

Figure 5. The effect of dasatinib on survival and disease progression in G93A mice. Rotarod activity, grip strength, body weight, and survival rate in G93A mice with or without dasatinib treatment (0, 5, 15, and 25 mg/(kg·day)). Survival of G93A mice was improved by dasatinib at a dose of 25 mg/(kg·day) compared with vehicle treatment (Log-rank test, $P<0.01$, 25 mg/(kg·day) vs. vehicle), whereas a lower dose of dasatinib (5 mg/(kg·day)) had no significant effect on life span. Weight loss was also ameliorated by dasatinib at a dose of 25 mg/(kg·day) compared with vehicle treatment (2-way ANOVA, $P<0.01$, 25 mg/(kg·day) vs. vehicle). The administration of dasatinib at 25 mg/(kg·day) similarly ameliorated grip strength (2-way ANOVA, $P<0.01$, 25 mg/(kg·day) vs. vehicle). The difference in physical function between the groups as assessed by rotarod was not significant by 2-way ANOVA, although a beneficial tendency of dasatinib was observed.
doi:10.1371/journal.pone.0046185.g005

Upregulation and activation of c-Abl in sporadic ALS

To investigate the implications of c-Abl in human sALS, we next examined the expression and activation levels of c-Abl in post-mortem spinal cord specimens from sALS cases. Lumbar spinal cord tissue from 3 sALS cases and 3 control cases with no neurodegenerative disease were used for immunohistochemical and western blot analyses. Western blotting revealed a more than 3-fold increase in c-Abl protein in sALS (Fig. 8A, B). More intense c-Abl immunohistochemical signal was also observed in lumbar spinal cord sections from sALS cases compared to control cases (Fig. 8C). Immunoreactivity of phosphorylated c-Abl (Tyr245 and Tyr412) in motor neurons was also increased in sALS specimens compared to controls (Fig. 8C). These findings indicate that upregulation and activation of c-Abl in motor neurons occurs not only in G93A mice but also in sALS patients.

Discussion

In this study, we established mouse motor neuronal cell lines in which either wild-type or mutant SOD1s were induced by doxycycline. We found that overexpression of mutant SOD1s induced expression and activation of c-Abl and decreased cell viability in a mouse motor neuron cell model. Furthermore, dasatinib, a BBB-permeable inhibitor of c-Abl, attenuated c-Abl phosphorylation and reduced the cytotoxicity induced by overexpression of mutant SOD1s. Dasatinib is a dual kinase inhibitor against c-Abl and c-Src family tyrosine kinases [31]. To clarify the specificity of c-Abl for the motor neuronal cytotoxicity, we performed cell proliferation and cell death assays with or without SU6656, which preferentially inhibits c-Src compared to c-Abl [32]. As shown in Fig. 3, dasatinib ameliorated the cytotoxic effects of mutant SOD1, whereas SU6656 did not. This finding indicates that c-Abl inhibition delays motor neuronal cell death caused by mutant SOD1. Our results are consistent with previous studies demonstrating that some apoptotic stimuli, such as amyloid beta and oxidative stress, also caused c-Abl activation [25,29], and that imatinib, another c-Abl inhibitor, had an inhibitory effect on apoptotic pathways [28].

Our study also provides evidence that c-Abl upregulation and activation occur in the lumbar spinal cord of G93A mice. c-Abl activation has recently been reported to occur in animal models of Niemann-Pick type C and Alzheimer's disease [28,33], but the present report is the first to demonstrate c-Abl activation in an animal model of ALS. Throughout the disease course of G93A